The Predicted Role of Stereospecificity in Crowding-mediated Effects on Reversible Association: A Brownian Dynamics Investigation

A Thesis
SUBMITTED TO THE FACULTY OF
UNIVERSITY OF MINNESOTA
BY

Joseph Daniel Powers

IN PARTIAL FULFULLMENT OF THE REQUIREMENTS
FOR THE DEGREE OF
MASTER OF SCIENCE IN BIOMEDICAL ENGINEERING

Adviser: David J. Odde, Ph.D.

August, 2013

ACKNOWLEDGEMENTS

I'd like to thank Dave Odde, for his dedicated advising, helpful comments, and for providing sufficient lab space and computational resources, Brian Castle, for his assistance in designing the model, as well as for his supportive advice, comments, and leadership, the entire Odde lab group, for their overall support and helpful comments, and the Minnesota Supercomputing Institute (MSI), for providing their high-performance computing resources.

ABSTRACT

Macromolecular crowding refers to the presence of inert molecules in close proximity to other reacting molecules, and is often discussed in the context of biochemical reactions in the cytoplasm. This phenomenon has been proposed to cause alterations in the intrinsic kinetics and thermodynamics of chemical reactions, which has led to certain undefined caveats when relating biochemical characteristics observed *in vitro* to those seen *in vivo*. In this work, the effects of macromolecular crowding were studied by means of a computational, Monte Carlo simulation using Brownian Dynamics, where generalized chemical association and dissociation reaction kinetics of varying degrees of stereospecificity were modeled both in the absence and presence of crowding molecules of different sizes. It was found that crowded environments impose energetic contributions to reactant pairs through depletion forces, which bias their translational and rotational diffusion in such a way that overall net assembly is favored, with stronger effects on reactants with higher degrees of stereospecificity than for those with low stereospecificity. These favorable forces are insufficient to overcome the slowing of translational diffusion by crowders for low stereospecificity reactions, but more than compensate for the translational slowing for high stereospecificity reactions. In general, the effects observed in the simulation are relatively modest, with k_{on} decreasing by 2-fold for low stereospecificity reactions, and increasing by 3-fold for high stereospecificity reactions. In addition, k_{off} decreases by ~30-60% in the presence of crowders (depending on the strength of the bond between the reactant pair), so that the equilibrium constant is increased by at most ~3.5-fold ($\Delta\Delta G^0 \cong -1.3 k_B T$). The moderate effects of crowding predicted in this work through strictly geometric constraints suggest that any effects observed *in vitro* larger than those found here are due to other energetic effects, such as solvent reordering. More generally, the results suggest that reactions in the cytoplasm are fundamentally insensitive to the physical presence of crowders over a large range of volume fractions (0-0.3).

TABLE OF CONTENTS

TABLE OF CONTENTS (*continued*)

LIST OF TABLES

LIST OF FIGURES

CHAPTER 1

INTRODUCTION

Macromolecular Crowding

The intracellular domain is a very complex and dynamic environment, comprised of nanometer-scale macromolecules diffusing throughout the cytoplasm, repeatedly colliding with one another, while their stochastic interactions provide an exchange of kinetic and thermal energy. What is less known, is how similar interactions with inert macromolecules might affect the reaction kinetics of biochemical macromolecules, and the detailed characteristics of the physical mechanisms of such interactions.

In terms of composition, the intracellular milieu consists of large amounts of proteins, nucleic acids, complex sugars, filament structures, and other large organelles, which collectively occupy a significant amount of cellular volume (Fulton, 1982). Although it is difficult to assign a value to the percentage of intracellular volume occupied by macromolecules, it has been estimated to be about 5-40% (Ellis 2001a; Ellis and Minton, 2003). This volume occupancy has been referred to as "crowded", rather than "concentrated", because no single macromolecule need be present at high concentrations for this effect to occur (Minton and Wilf, 1981; Minton, 2001), and, although it is common for this phenomenon to be referred to as the "excluded volume

effect", such a title might imply misleading ideas, for reasons discussed below. Therefore, this phenomenon shall be referred to in this work as "macromolecular crowding" or, more simply, "crowding".

In recent years, the idea of macromolecular crowding has become of increasing interest to biochemists when studying biochemical reactions *in vitro*. Discrepancies observed between reaction kinetics, thermodynamics, and diffusive characteristics of macromolecules measured *in vivo* with those measured *in vitro* raised more questions than answers, and triggered a large investigation for possible causes. For example, Banks *et al*. reported a ~3-fold drop in the diffusion coefficient of streptavidin in a solution of 1.08kDa dextran at a 0.25 volume fraction (Banks & Fradin, 2005). Additionally, Kozer and Schreiber observed a decrease in the diffusion-limited association rates of the β-lactamase (TEM)- β-lactamase inhibitor protein (BLIP) with the addition of crowding molecules, as compared to rates observed in buffer solutions (Kozer & Schreiber, 2004). Lindner *et al*. also reported a ~3-fold increase in the association rate constant of human spectrin heterodimers in the presence of 10% w/v concentration of dextran, and, similarly, over a ~2-fold increase in the association rate constant for actin polymerization in the presence of 15%w/v concentration of dextran (Lindner & Ralston, 1995). Clearly, macromolecular crowding caused noticeable effects in experimentation, but the details of why and how it occurred remained nebulous.

In the early 1980s, Allen Minton proposed several arguments as to how crowding can increase association rates and equilibrium constants by *orders of magnitude* through a

theoretical approach investigating the changes in thermodynamic activity coefficients of reactants as a function of excluded volume (i.e. volume occupied by crowding molecules, no longer accessible to reactants) (Minton & Wilf, 1981; Minton, 1983; Minton, 1997; Zimmerman & Minton, 1993). Minton's initial predictions raised many questions as to whether or not reactions studied *in vitro* should be compared to those *in vivo* without some sort of treatment of crowding (Ellis & Minton, 2003; Minton, 2006), and, if such precautions are necessary, how they should be treated.

In particular, researchers have begun to investigate the effects of crowding on various *in vitro* experiments, such as protein folding and aggregation, bimolecular association rates, actin polymerization (Frederick *et al*. 2008), ligand/receptor binding rates, microtubule assembly (Wieczorek *et al*., 2013), and many others. Recently, results of many experimental efforts with regards to crowding have suggested that some of Minton's initial predictions might have been an overestimation (Phillip & Schreiber, 2013). Therefore, the question of whether or not crowding should be accounted for (and, if so, how) when studying reactions *in vitro* still stands.

Depletion Forces in Crowded Environments

As early as the 1950's, the physical mechanisms involved within crowded solutions were being studied. Asakura and Oosawa derived theoretical predictions describing energetic consequences of molecules diffusing in a crowded environment due to local fluctuations in entropy (Oosawa, 1954; Asakura & Oosawa, 1958). They found

that there is an increase in entropy in the system when molecular pairs come in close enough proximity such that other molecules cannot be placed between them, producing a force acting radially inward on the pair, which biases their translational diffusion toward one another.

Yodh *et al*. reproduced this effect experimentally by studying the separation distances between test pairs of molecules under different crowding scenarios (Yodh *et al*., 2001). They found that these depletion forces induce negative (favorable) energy of roughly $1k_BT$ (where k_B is Boltzmann's constant and T is the absolute temperature) on rods and spheres approaching one another for relatively low concentrations of crowders.

Clearly, depletion effects are an important aspect of crowded environments that must be considered when investigating association and dissociation kinetics of biomolecules in the cytoplasm. However, there has been little discussion of how changes in the energetic landscape felt by pairs of molecules in crowded media affect their reaction kinetics, leaving the significance of these effects undefined in terms of their relevance to how biomolecular reactions in crowded, *in vivo* studies differ from reactions in uncrowded, *in vitro* studies.

Monte Carlo Methods & Brownian Dynamics

Given modern advancements in computational capabilities, recent studies have focused on computational simulations using Brownian Dynamics to examine the changes in diffusion patterns and reaction rates as functions of the volume occupied by

crowders (Phillip & Schreiber, 2013; Kim & Yethiraj, 2009; Kim & Yethiraj, 2010; Wieczorek & Zielenkiewicz, 2008). In general, Brownian dynamics is a well-established, reliable method for modeling the Brownian (random) motion of molecules (Metropolis & Ulam, 1949), derived through a simplification of the Langevin Dynamics approach by assuming there are no inertial effects in the system. Using these methods enables one to investigate changes in diffusion characteristics, as well as the reaction kinetics and thermodynamics, of biomolecules in the presence of crowding.

In many cases, the chosen tool for creating such models is an approach called the Monte Carlo method, a type of computational algorithm which relies on multiple generations of pseudo-random numbers to obtain a specific numerical outcome—an especially useful tool when studying the random, Brownian motion that drives the diffusion of particles. In Monte Carlo simulations, information from a current state is used as the input to calculate, according to the appropriate probabilistic rates, the next system state, thus creating a history-dependent model of events in space and time. For example, a molecule's current position and orientation in space can be used as information to determine the molecule's upcoming translation and rotation. More specifically, random numbers can be generated for the molecule's x-, y-, and z-coordinate translation, as well for as its rotation about the x-, y-, and z-axes (in the laboratory reference frame), and added to its previous position, resulting in one time step in three dimensions. This process can be repeated multiple times, resulting in a realistic simulation of molecular diffusion.

Like the *in vitro* experiments discussed earlier, the past few years have been a bourgeoning time for scientists studying macromolecular crowding using computational methods. For example, Wieczorek and Zielenkiewicz, developed a computational model, using Brownian Dynamics methods, with which protein-protein associations were modeled (Wieczorek & Zielenkiewicz, 2008). Their model represented a range of spherical crowding molecule sizes (relative to the spherical reactant size), as well as an incorporation of the diffusion-limited condition for generic protein-protein associations. They reported a ~2-fold drop in the diffusion-limited association rate constant for crowding agents of equal radii to that of the reactant molecules, and a ~1.3-fold drop for larger-sized crowding molecules (5/3 times larger radii than the reactants). However, when Wieczorek *et al*. simulated an atomically detailed model for the association of a hen egg lysozyme with the HyHEL antibody, they reported a ~2.7-fold *increase* in the association rate with crowding— a much lower-probabilistic reaction than the diffusion-limited case. However, exactly how crowding was affecting the reaction kinetics was still unclear because of their use of an atomically detailed case for only one particular pair of non-spherical reactants only provides predictions for this one particular case. A more robust, generalized model (i.e. not specific to a particular antibody-antigen pair) examining the predicted effects of crowding would enable further comparisons to a greater variety of cases and a more fundamental understanding of the consequences of crowding for reversible association-dissociation reactions.

More recently, Kim *et al*. developed a more generic computational model with which they explored changes in the relative on-rate constants for pseudo-first-order reactions with increasing volume fractions of crowding agents, using a Brownian Dynamics approach (Kim & Yethiraj, 2009). The group simulated biochemical reactions in crowded solutions by altering the probability of undergoing a reaction during an encounter such that some cases had a very low probability of reacting (0.001), whereas others had a very high probability of reacting (1.00, for the diffusion-limited case) upon an encounter. They found that the lower probability reactions produced a ~2.5-fold increase in relative association rates, and a ~2-fold reduction for the diffusion-limited case as the crowder volume fraction increased from 0.0 to 0.4. However, it can be argued that the reaction probability of diffusing reactants is not constant in time (i.e. is history-dependent). Inherent to biological reactions, the probability of undergoing a reaction depends on previous failed attempts to react and the rotational correlation of the reactants while in close proximity to one another (discussed in detail in The Role of Stereospecificity, below). This history dependence is not addressed in this group's model due to their assumption of a uniformly reactive surface on their spherical reactants, thus, perhaps, not accurately capturing important details within stereospecific reactions under crowding (Qin *et al.*, 2012).

The Role of Stereospecificity

Even with such efforts to model the effects of macromolecular crowding, there has yet to be a comprehensive model which captures the effects due to variable crowder densities and sizes relative to the reactants, while including rotationally dependent reaction criteria (stereospecificity) and potential energy considerations. Stereospecificity is an important detail to consider when studying macromolecular crowding, as it describes the rotational restrictions most biomolecules have to meet when undergoing association, as proposed in a computational model of protein-protein associations by Northrup and Erickson (Northrup & Erickson, 1992). In part, the history-dependent probability of a reaction during an "encounter" between two reactants (i.e. when they are sufficiently close to each other that they could potentially form an association) can be thought of as related to the stereospecificity associated with each reaction, thus creating a *conditionally probabilistic* reaction. The idea of conditional probability arises when considering that the relative rotational orientation of reactants at one encounter contributes to the probability of the reactants experiencing a reaction at subsequent encounters, essentially creating a history-dependent, non-constant probability of reacting at any given encounter. An encounter can be roughly defined as when the reactants diffuse to a close enough proximity such that if they were properly aligned, they would form a bond. Therefore, based solely on geometry, each reactant has a certain intrinsic probability of reacting with another reactant on their first encounter. If, however, on that first encounter the reactants do not form a bond, then the probability

that they form a bond on their second encounter is extremely unlikely, and, in fact, much *less* probable than that of their first encounter due to their relative rotational configurations likely being highly uncorrelated. Therefore, the reactants are more likely to diffuse apart after their first failed attempt to form a bond rather than remain in close proximity exploring different rotational configurations until a binding event occurs.

Northrup and Erickson developed a computational model in which they addressed the importance of including stereospecificity while simulating protein-protein association rates (Northrup & Erickson, 1992). They reported that stereospecificity leads to association rate constants that are well below the Smoluchowski limit (~1000-10,000$\mu M^{-1}s^{-1}$), but in agreement with experimental data for many protein-protein association reactions (~1-10$\mu M^{-1}s^{-1}$). They simulated stereospecificity by assigning four "contact points" lying on a plane tangential to the surface of spherical reactants, and defining a range of stereospecific reactions as when N = 0, 1, 2, or 3 contact points on one reactant became aligned (separated by <0.2nm) with the corresponding contact points on another reactant (see Stereospecificity in Chapter 2, below). However, they did not examine how the presence of crowding molecules would influence the association or dissociation rate constants of such stereospecific reactants.

In general, the crowder-modeling field has yet to address the issue of stereospecificity at the level detail proposed by Northrup and Erickson's computational simulation. As stated above, the Wieczorek and Zielenkiewicz model included the stereospecific antibody-antigen binding case (Wieczorek & Zielenkiewicz, 2008), but

lacks the generality of Northrup and Erickson's model, whereas the *ad hoc* probability of reacting upon any given encounter used by Kim and Yethiraj (Kim & Yethiraj, 2009) does not capture the potential influences of stereospecificity in crowded environments (Qin *et al.*, 2012). In addition, neither computational model addresses changes in dissociation kinetics with the addition of crowding molecules.

The Northrup and Erickson model provides a generalized, robust framework for studying the dependence of association reaction kinetics on stereospecificity in the absence of crowders, and, in principle, can be extended to dissociation rate kinetics to obtain a complete thermodynamic analysis of reversible association. The idea here is to use the generic framework developed by Northrup and Erickson to create a novel, stereospecific-dependent model of biochemical reaction kinetics and thermodynamics in the presence of crowding molecules.

Model Objectives

The purpose of this study is to elucidate the effects of macromolecular crowding on reaction kinetics for reactants with varying degrees of stereospecificity as a function of increasing crowder volume fraction, as well as of varying crowding molecule sizes relative to the reactants, through developing a generalized, robust computational model. The results of this model should describe, in detail, how macromolecular crowding affects the association and dissociation kinetics of various stereospecific biomolecules by capturing the intrinsic physics and thermodynamics embedded in these interactions at

the molecular level. The model should also be able to accurately reproduce results and observations made by others for similar experimental or computational situations, while remaining general enough such that changes in the parameter set of the model can be made to address other questions not previously answered. Lastly, the model should provide valuable insight as to if and/or how macromolecular crowding should be treated when studying biochemical reactions *in vitro*. By developing a firmer theoretical understanding of how biomolecules behave in crowded environments, we can predict how these behaviors might influence biological processes.

CHAPTER 2

METHODS

To investigate the theoretically expected effects of macromolecular crowding on the association and dissociation rates of two macromolecular reactants, a Brownian Dynamics simulation was developed, creating a three-dimensional, spatiotemporal model. A variety of crowding scenarios were investigated, providing a comprehensive characterization of the role of macromolecular crowding on biochemical reaction kinetics and thermodynamics.

Overall Computational Model

Model Parameters

All molecules in the simulation were treated as hard spheres with infinite repulsion at their surfaces. The nonspecific steric repulsion is described as a piecewise-defined potential energy function based on the spheres' relative radial separation distances, *r*, with respect to their centroids, as in Eq. 1.

$$U(r)=\begin{cases}\infty, & r \le R_r + R_c \\ 0, & r > R_r + R_c\end{cases} \quad (1)$$

Reactants had radii (R_r) of 1.8nm, a parameter initially proposed in Northrup and Erickson's model (Northrup & Erickson, 1992), whereas crowding molecules, or "crowders", had radii (R_c) ranging from 0.85 times the reactant radius, equal to, or 1.25

times (1.53nm, 1.8nm, and 2.25nm, respectively). Each simulation trajectory consisted of two reactants in a 16x16x16nm (4.096×10^{-21}L) box (simulation domain), resulting in a concentration of 0.405mM, and were surrounded by a homogeneous composition of crowding molecules of one of the varying sizes described above. This range in crowder size allowed for the effects due to crowding to be investigated as a function of relative crowder size.

All molecules were assumed to be placed in a continuum solvent of room-temperature water— a valid assumption for molecules sufficiently larger than that of the solvent (Hall & Minton, 2003).

Initial Molecular Placement

Reactants were initially placed in the simulation domain at random locations either in a bound state (when simulating dissociation), or randomly oriented (when simulating association). The reactants were allowed to be placed up to one radius-length outside the box, such that their centroid positions were contained inside the box at all times. Crowding molecules were placed among the reactants at random locations while avoiding overlap with any other molecule in the system, but were allowed to be placed such that their centroid positions could be up to one crowding radius outside the box. This was done to minimize the depletion effects at the boundaries of the box, as well as to more closely resemble the Poisson distribution associated with taking a

random sample of macromolecules from an arbitrary intracellular domain. A depiction of these initial placement constraints is shown in Figure 1.

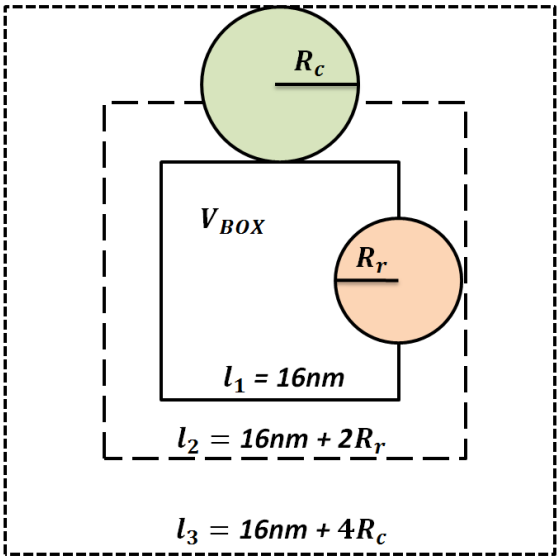

Figure 1. *Diagram of the criteria for the initial placement of molecules and boundary conditions. Reactants were allowed to be placed up to one radius (R_r) outside box, whereas crowding spheres were allowed to be placed up to 2 radius-lengths ($2R_c$) outside the domain.*

Boundary Conditions

Since this model relies on maintaining a constant volume fraction (ϕ) of crowding molecules in the simulation, reflective boundary conditions along the walls of the cubic domain were implemented. If a crowding molecule were to take a step resulting in its centroid being more than one radius-length in the *x*-, *y*-, or *z*-direction outside of the box, the crowding sphere would then take a step in the corresponding *x*-, *y*-, or *z*-coordinate of equal magnitude, but in the opposite direction (i.e. perpendicularly away from the wall). This allowed the crowding spheres to step almost completely out of the box before being reflected into the domain. If, however, the reflection resulted in

an illegal overlap with another molecule, the crowding sphere was brought back to its previous *legal* position (i.e. *not* back outside the box), and a new random step was generated for that molecule. Similarly, the reactants were reflected away from the walls in the same manner if their centroids attempted to step out of the domain, and followed the same overlapping guidelines. Figure 1 again depicts these constraints, as they are the same as for the initial placement of molecules in the domain.

Volume Fraction

Next, the volume fraction of the molecules in the system was determined to serve as an independent variable in the model. The volume fraction is a dimensionless quantity describing the amount of volume occupied by the crowding molecules at any given time. It is important to note that, although there is a loss of volume in the box at any single moment of time by inserting crowders, every molecule still has some probability of exploring every unit of space in the domain (due to diffusion) given a long enough duration of time. Therefore, the term "volume fraction" does not refer to some finite "accessible" volume to the reactants, but is, rather, a metric to quantify the *average* amount of volume in the domain being occupied by crowders over the duration of the simulated time.

A naïve approach to calculating the volume fraction would be to use simple geometric ratios of the volume of the box and the total volume of crowding molecules inside the box. However, one would find that using such a method would result in

significantly underestimated values for the volume occupancy of the crowding spheres actually contained inside the box due to the initial placement criteria and boundary conditions for each molecule (see Figure 1). Therefore, the volume fraction was determined by defining a grid throughout the domain (Figure 2a), and calculating the distance, L, that every grid-point was separated from each crowding sphere's centroid, and summing those that were within R_c from a crowder centroid (Eq. 2), providing a total (summed) crowder volume contained within the box at any moment in time. In the limit of filling the box with infinitely-many grid-points, this method would yield an exact value for the fraction of volume of the box consumed by the crowding spheres at any single time point. Here, a grid of $n = 10^6$ points was used (100^3), and an average over multiple runs was taken to determine the mean volume fraction, ϕ, as a function of the number of each of the three sizes of crowding spheres (Figure 2b).

$$\phi = \frac{1}{n_{tot}} \sum n\Big|_{L<R_c} \tag{2}$$

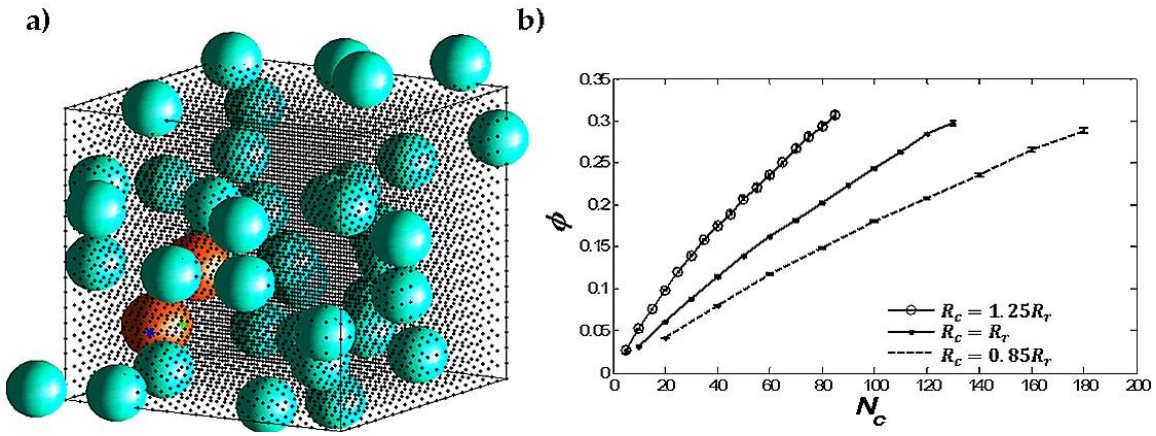

Figure 2. *Volume fraction description.* ***a)*** *Depiction of the grid method used to determine the volume fraction occupied by the crowding molecules. The number of grid-points shown above is* 20^3 *for clarity, however,* 100^3 *grid-points were used when calculating* ϕ *in the model.* ***b)*** *Calculated volume fraction,* ϕ*, as a function of the number of crowding molecules,* N_c*.*

Stereospecificity

As initially proposed by Northrup and Erickson's protein-protein association model, on each reactant sphere, four contact points, or zones, were assigned to a plane lying tangential to the surface of the reactant, creating a ~1.7 x ~1.7nm "reactive patch" for each reactant (Figure 3a) (Northrup & Erickson, 1992). These four zones lying on the tangential plane provided a rotational constraint as the reactants now needed to be oriented properly relative to one another to undergo a reaction (for reactions other than the diffusion-limited type).

As in the Northrup and Erickson model (Northrup & Erickson, 1992), stereospecificities were defined as an N = 0, 1, 2 or 3 reaction, where N is the number of zones on one reactant coupled with the corresponding zones on the other reactant. More explicitly, an "N = 0 reaction" occurred if the surfaces of the reactants came within

2Å of one another, irrelevant of rotational conformation (i.e. the "N = 0" case is synonymous with the "diffusion-limited" case, or the "Smoluchowski" limit (Smoluchowski 1971)), whereas an "N = 1 reaction" was said to occur if one pair of zones (red-to-red, for example) came within 2Å of one another. Understandably, an "N = 2 reaction" and an "N = 3 reaction" were defined as two pairs (red-to-red *and* blue-to-blue, for example), or three pairs of zones coming within 2Å, respectively. An example of reactants in an N = 2 conformation is shown in Figure 3b, below. In general, the higher the value of N, the greater the extent of stereospecificity that is required for the reactants to undergo a reaction. Each of these stereospecific requirements were initially proposed by Northrup and Erickson's protein-protein association model (Northrup & Erickson 1992).

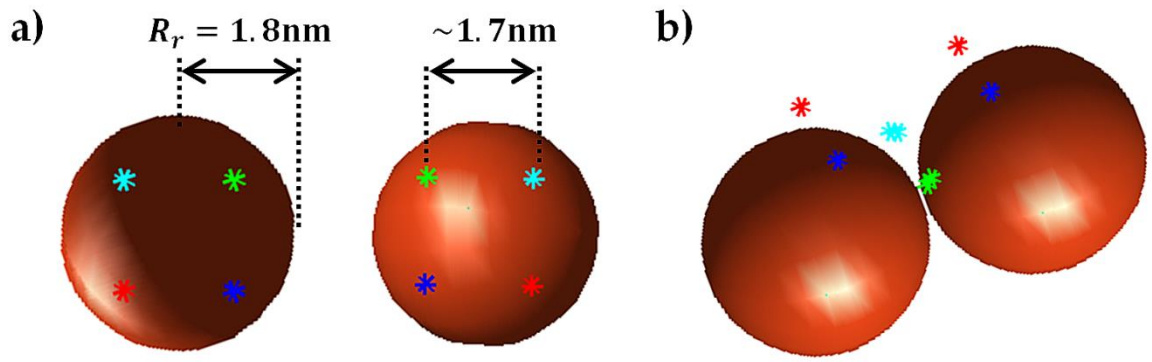

Figure 3. *Description of reactant molecules and their stereospecificities.* ***a)*** *Dimensions of reactant spheres, and the "reactive patch" assigned to each sphere. The patch was defined as four zones, arranged in a ~1.7x~1.7nm square, lying on a plane tangential to the surface of the sphere.* ***b)*** *Example of an N = 2 conformation. The green and turquoise zones on each reactant are within 2Å of one another. These model parameters were initially proposed by Northrup and Erickson* (Northrup & Erickson, 1992).

Molecular Diffusion & Variable Time Step

All translational and rotational molecular diffusion was simulated using a modified, Metropolis Monte Carlo method (Metropolis & Ulam, 1949) to update the molecular positions after each time step, *j*, as

$$(x, y, z)^{(j)} = (x, y, z)^{(j-1)} + \boldsymbol{\delta}(\tau) \tag{3}$$

and molecular orientations, as

$$(\rho, \theta, \psi)^{(j)} = (\rho, \theta, \psi)^{(j-1)} + \boldsymbol{\delta}(\tau) \tag{4}$$

where $\rho, \theta,$ and ψ are rotational orientations relative to the *x*-, *y*-, and *z*-axes, (in the laboratory reference frame) respectively, and τ is the increment of time for a diffusive step. The terms on the left represent each molecule's new position and orientation in space, whereas the first terms on the right are each molecule's previous location and orientation in space. The second term on the right, $\boldsymbol{\delta}(\tau)$, is a vector quantity of random numbers sampled from a Gaussian distribution, where each element has characteristics

$$\left\langle \delta_i(\tau) \right\rangle = 0, \quad \left\langle \delta_i^{\,2}(\tau) \right\rangle = 2D_{T,r}\,\tau = 2D_{T,c}\tau \ , \tag{5}$$

$$\left\langle \delta_k(\tau) \right\rangle = 0, \quad \left\langle \delta_k^{\,2}(\tau) \right\rangle = 2D_R\,\tau \tag{6}$$

where i = *x*, *y*, or *z*, and k = ρ, θ, or ψ. The terms $D_{T,r}$ and $D_{T,c}$ are the translational diffusivities for reactants and crowders, respectively, and D_R is the rotational diffusivity for reactants, based on the Stokes-Einstein-Sutherland equations for a sphere,

$$D_{T,r} = \frac{k_B T}{6\mu\pi R_r} \quad , \quad D_{T,c} = \frac{k_B T}{6\mu\pi R_c} \tag{7}$$

$$D_R = \frac{k_B T}{8\mu R_r^3} \tag{8}$$

where k_B is Boltzmann's constant, $T = 298.15K$, and $\mu = 8.91x10^{-4}(N \cdot s)/m^2$.

The updated angles of rotation after each step were then used in traditional rotation matrices (Eq. 9) to apply the new three-dimensional rotation to each reactant, as in Eq. 10 and 11 below. It should also be noted that rotation was ignored for crowding molecules, as it was an unnecessary detail for the purposes of this model.

$$\boldsymbol{R}_x = \begin{bmatrix} 1 & 0 & 0 \\ 0 & \cos\delta_\rho & -\sin\delta_\rho \\ 0 & \sin\delta_\rho & \cos\delta_\rho \end{bmatrix}, \boldsymbol{R}_y = \begin{bmatrix} \cos\delta_\theta & 0 & \sin\delta_\theta \\ 0 & 1 & 0 \\ -\sin\delta_\theta & 0 & \cos\delta_\theta \end{bmatrix}, \boldsymbol{R}_z = \begin{bmatrix} \cos\delta_\psi & -\sin\delta_\psi & 0 \\ \sin\delta_\psi & \cos\delta_\psi & 0 \\ 0 & 0 & 1 \end{bmatrix} \tag{9}$$

$$\boldsymbol{M}^{(j)} = \boldsymbol{M}^{(j-1)} \boldsymbol{R}_x \boldsymbol{R}_y \boldsymbol{R}_z \tag{10}$$

The matrix $\boldsymbol{M}^{(j)}$ is a three-dimensional rotation matrix that defines the overall rotation of the reactants about the laboratory reference frame, and is updated after every time step, *j*. Therefore, the combination of Eq. 3, 4, 9 and 10 yields the total translational-rotational movement taken by the reactants at every step, as

$$(x, y, z)^{(j)} = \boldsymbol{M}^{(j)} (x, y, z)^{(j-1)} + \boldsymbol{\delta}(\tau) \quad . \tag{11}$$

To optimize the simulation run-time by minimizing the number of translational displacements taken by each molecule, a variable time step was derived, which varied as a function of the overall minimum center-to-center distance, *d*, of any two molecules in the system, unless the reactants were in some bound conformation (i.e. in any of the *N* conformations discussed above), for which case the time step was fixed at 0.2ps. The

variable time step was derived using the root mean squared displacement (*RMSD*) of two diffusing spheres in three dimensions at any given time step, and relating it to *d*, as

$$RMSD = \sqrt{6(2D_T)\tau} = \frac{d}{\lambda} \tag{12}$$

where λ is an adjustable optimization parameter determined based on the amount of detail required per step (a more demanding stereospecificity, i.e. higher N, required finer rotational and translational steps when the reactants were in close proximity). For the diffusion-limited (N = 0) and N = 1-3 cases, it was found that λ = 5 and λ = 20, respectively, were sufficient values to reach other predicted on-rate constant values (Northrup & Erickson 1992) (see Table A3). It should be noted that the factor of 2 multiplied by the diffusion coefficient is a correction factor to account for the fact that both spheres of interest were diffusing. Therefore, the variable time step, τ, was recalculated after every diffusive step, using

$$\tau = \frac{1}{12D_T}\left(d/\lambda\right)^2 \tag{13}$$

It should be noted that there was no distinction between reactant molecules and crowding molecules for the purposes of this calculation.

On-rate Simulation

Far-field & Near-field Regimes

Using this model, simulations became very computationally expensive with increasing volume fractions of crowding molecules, and, therefore, became very time-consuming. This is because the pair-wise checks required to ensure there were not any spheres overlapping with one another after each translational step increased non-linearly with the number of molecules in the system. Consequently, the total simulation time scaled as a higher-order polynomial with the number of crowding spheres in the system (see Data Analysis section, below, for an example of the scaling). To combat this, the model was broken down into two regimes: a far-field regime and a near-field regime.

The far-field regime was considered to be when the reactants were separated by a center-to-center distance of 4.2 nanometers or greater, and the near-field regime was considered to be when the reactants were separated by a center-to-center distance less than 9 nanometers. More specifically, the far-field regime was treated by placing each pair of reactants at an initial separation distance of 9 nanometers, center-to-center, and terminating the trajectory when the reactants became separated by a distance of 4.2 nanometers, center-to-center. A diagram depicting this treatment is shown in Figure 4. In the far-field regime, reactant orientation was not accounted for, as each trajectory was terminated prior to the reactants being in close enough proximity to undergo a reaction of any type with any reasonable probability (<0.003), making this portion of the model

much more computationally efficient. Additionally, terminating the trajectory at reactant separation distances of 4.2 nanometers essentially simulates a diffusion-limited case, thus enabling the larger variable time step to be utilized (λ = 5), further decreasing the computational run-time. Depending on the volume fraction of crowding spheres used, either 100,000 or 50,000 trajectories were run to comprise the distributions of the far-field diffusion times (i.e. the time to diffuse from 9nm to 4.2nm, center-to-center). These distributions of diffusion times were saved and reused for the near-field simulation, as discussed in the following section, and the rates of arrival to a separation distance of 4.2nm (from 9nm) were recorded as k_{DIFF}, as shown in Figure 4.

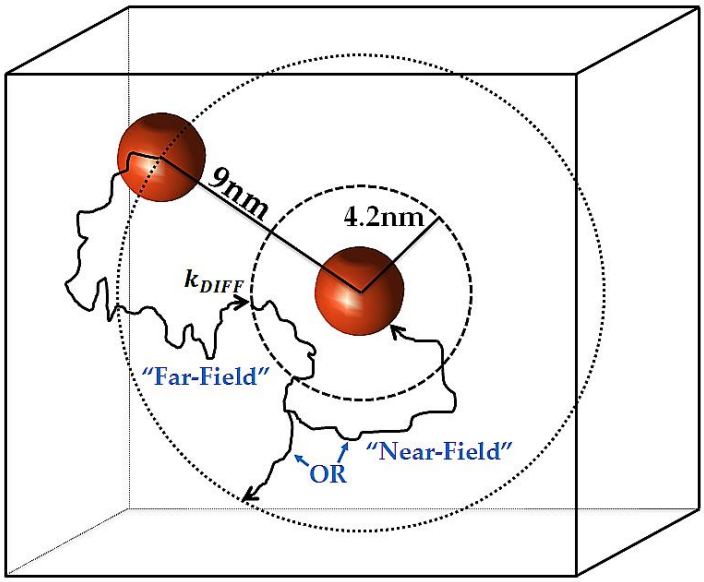

Figure 4. *Diagram of the far-field and near-field regimes. The far-field regime was considered to be when reactants were separated by a center-to-center distance greater than 4.2 nanometers after having started at a center-to-center distance of 9nm. The rate of arrival to 4.2 nanometers after starting from 9 nanometers was defined as* k_{DIFF}*. The near-field regime was considered to be when reactants were separated by a distance less than 9 nanometers, center-to-center, after having started at 4.2nm. While in the near-field regime, if reactants diffused back to 9nm, they were instantaneously placed back at a distance of 4.2nm (as discussed above), but if the reactants associated (N=0 conformation shown), the trajectory was terminated (as discussed below).*

The near-field regime was initiated by placing reactants at a center-to-center separation of 4.2nm (the *termination* distance for the far-field regime), with randomly oriented rotations relative to one another. All crowding spheres were then randomly redistributed within the domain, following all placement guidelines discussed above. Now, however, if the reactants diffused back to a center-to-center distance of 9nm (the *initial* distance of the far-field simulation), a random sample from the exponentially distributed far-field diffusion times was added to the near-field diffusion time to reach that 9nm separation distance. This provided a pseudo-continuum between the far-field regime and the near-field regime, as the *total* diffusion time was required for determining the on-rate constant. This process was repeated multiple times, collecting data for any $N = 0$, 1 and 2 conformations that happened to occur prior to reaching an $N = 3$ conformation, at which point the trajectory was terminated and the cumulative diffusion time to achieve each conformation was recorded.

The near-field simulations required much higher levels of detail regarding the translational and rotational diffusion, since the reactants needed to diffuse to the proper, specific orientation (e.g. $N = 3$) prior to each trajectory's termination. Therefore, as stated above, a value of $\lambda = 20$ was used for the variable time step in the near-field simulation.

Potential Energy Consideration

Once reactants reached an $N = 2$ conformation, they began stepping on a square-well potential with a depth of -4.2*kcal*/*mol* (or about -7.1k_BT), a value initially used in

Northrup and Erickson's model based on generally accepted bond strengths for protein-protein interactions of the types being modeled (Northrup & Erickson 1992). They also assumed no appreciable energetic contribution for reactants in the N = 1 conformation. Thus, the conformation-dependent, piecewise-defined potential energy function, $U(N)$, is described in Eq. 14, and illustrated in Figure 5.

$$U(N) = \begin{cases} \infty, & Overlap \\ -18.6k_BT, & N = 3,4 \\ -7.1k_BT, & N = 2 \\ 0, & N = 0,1 \end{cases} \tag{14}$$

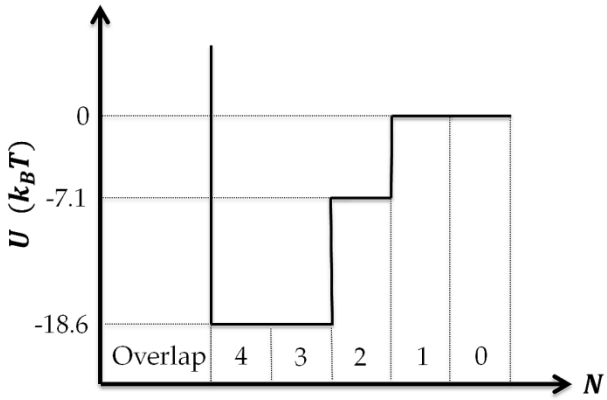

Figure 5. *Potential energy diagram describing the energetic interaction between reactants as a function of the number of coupled zones, N. To completely bind, reactants had to reach an N = 3 conformation, although intermediate partial bonds were also recorded.*

With each Brownian step taken in the N = 2 conformation, the probability, P, of breaking both, or either, of the two zones was defined according to Boltzmann's Law, as,

$$\frac{P(N=2)}{P(N=0,1)} = \exp(-7.1k_BT) \equiv K_{eq}^{(2\rightarrow 0,1)} \quad . \tag{15}$$

If an attempt to break this bond was rejected, the step was refused, time was advanced, and the bond remained intact.

Finally, the mean diffusion time for the reactants to bind (i.e. the time needed to reach a reactive conformation of N = 0, 1, 2, or 3), was used to calculate the overall association rate constant for each conformation, $k_{on,N}$, using

$$k_{on,N} = \frac{1}{\langle t_{B,N} \rangle C_r} \quad [=] \quad M^{-1}s^{-1} \tag{16}$$

where C_r is the reactant concentration (0.405mM) and $t_{B,N}$ is the diffusion time prior to binding in either an N = 0, 1, 2, or 3 conformation, depending on the stereospecific definition of the reaction.

Off-rate Simulation

The off-rate simulation began with the reactants in a bound state, and randomly positioned in the simulation domain. The bimolecular complex was also randomly oriented, and the crowding spheres were then placed randomly among the bound reactants, following the initial placement and overlap criteria discussed above. With every Brownian step taken while in the N = 3 conformation, the probabilities associated with breaking part of, or all of, the bond were now given values

$$\frac{P(N=3)}{P(N=2)} = \exp(-11.5k_BT) \equiv K_{eq}^{(3\to 2)} \tag{17}$$

and

$$\frac{P(N=3)}{P(N=0,1)} = \exp(-18.6k_BT) \equiv K_{eq}^{(3\to 0,1)} \tag{18}$$

per Eq. 14, and the probability of going from an N = 2 conformation to an N = 0 or 1 conformation was the same as for the binding case (Eq. 15).

An arbitrary intrinsic bond strength had to be chosen such that the computational expense for running the dissociation simulation was not too great, and such that the simulation would yield generally excepted values for bimolecular reaction thermodynamics. Therefore, an overall bond strength of $-18.6k_BT$ was selected, as it is well within the range of published values for the intrinsic bond strength of protein-protein bonds (Howard 2001). It was also assumed that the changes in energy between the $N = 3$ and $N = 4$ or $N = 0$ and $N = 1$ cases are negligible compared to that between the $N = 2$ and $N = 3$ or $N = 1$ and $N = 2$ cases (e.g. the rotational orientation required for the reactants to be in an $N = 3$ configuration is very similar to that of the $N = 4$ case, thus not imposing a significant additional entropic penalty).

Determining when the reactants were officially unbound could not simply be treated as when all four zones were separated by a distance greater than 2Å. This is due to the fact that, when the reactants first separate, their relative orientations are still highly correlated, thus increasing the probability that they will soon re-associate. Therefore, reactants were assumed to be completely unbound only once they had again reached the far-field regime, where their centroid separation distance is at least 9 nanometers. Simulating association and dissociation enabled a complete analysis of the thermodynamics during the process of reactants beginning in the far-field regime, diffusing into the near-field regime, binding, unbinding, and diffusing back out to the far-field regime.

Next, the off-rate constants were calculated in a similar way as in Eq. 16, in that the total diffusion time to unbind from an *N*-bound state, $t_{U,N}$, was monitored and saved. The inverse of the average diffusion time to unbind was taken as the off-rate constant, as

$$k_{off,N} = \frac{1}{\left\langle t_{U,N} \right\rangle} \quad [=] \quad s^{-1} \qquad . \tag{19}$$

Thermodynamic Considerations

Due to the nature of the simulation, the standard Gibbs free energy for the association of an *N*-conformation (ΔG_N^o) could easily be broken up into two main contributors, as

$$\Delta G_N^o = -k_B T \ln\left(\frac{k_{on,N}}{k_{off,N}}\right) = \Delta G_{S,N}^o + \Delta G_{B,N}^o \tag{20}$$

where $\Delta G_{B,N}^o$ is the intrinsic bond energy for reactants in conformation, *N*, and $\Delta G_{S,N}^o$ is an entropic penalty—a positive value which encompasses the loss of translational and rotational freedom of the reactants due to binding.

Lastly, the intrinsic bond strength of the reactants is an average of the potential energy, weighted by the time, *t*, spent diffusing in the various stages of the overall potential well. Therefore, the intrinsic bond energy was calculated as the time-averaged potential energy using

$$\Delta G_{B,N}^o = \frac{1}{m}\sum_{i=1}^{m}\left(\sum_{j=1}^{n} U^{(j)} \frac{t^{(j)} - t^{(j-1)}}{t_i^{(n)}}\right) \tag{21}$$

where m is the number of trajectories simulated, and n is the number of steps taken by the reactants prior to completely unbinding (i.e. i is any one trajectory, and j is a completed diffusional step taken by the reactants within one trajectory). It should be noted that this calculation included the diffusion time it took for the reactants to diffuse to a center-to-center distance of 9nm after fully breaking all four zones. However, the added time to reach the far-field regime is negligible compared to the total time spent diffusing in some bound conformation. To ensure that the added time for reactants to go from the $N = 0$ state to a 9nm center-to-center separation distance was not biasing the weighted average for the intrinsic bond strength, this extra duration of time was monitored and compared to the total time needed to completely unbind, and was found to be less than one percent of the total simulated time.

Data Analysis

Since the diffusion times for these stochastic processes fit an exponential distribution, an inordinate amount of computational time was required to simulate those points lying far out on the tail of the distribution. Therefore, an estimate for the mean value of the distribution was established using binomial theory and exponential distribution statistics, as follows.

First, ~30 trajectories were run to completion, providing an initial distribution and estimate for the mean time (τ_E) for an event to occur. This initial distribution was then fit to an exponential distribution of equal mean to ensure it was, indeed,

exponential (p>0.15 in a Kolmogorov-Smirnov test). Next, 200 trajectories were run until the total simulated time reached that mean value (τ_E) regardless of whether or not a binding or unbinding event had occurred. The probability, p_E, that an event had occurred was calculated as the number of successes, κ_E, out of the total number of trajectories, m (the subscript E is defined as any specific event; $E \equiv N$ = 0, 1, 2, or 3 for a binding event, or $E \equiv U$ for an unbinding event). This probability was then used to define the probability density function (*PDF*) for the exponential distribution, as

$$\frac{\kappa_E}{m} = p_E = 1 - \exp(-\lambda_E \tau_E) \tag{22}$$

where λ_E is the rate of the distribution. Solving for λ_E yields

$$\lambda_E = \frac{\ln(1 - p_E)}{-\tau_E} \quad [=] \quad s^{-1} \tag{23}$$

which serves as the most probable estimate for the inverse of the mean diffusion time for an event to occur in any given simulation. Therefore, these values were substituted into Eq. 16 and 19 for $1/\langle t_{B,N} \rangle$ and $1/\langle t_{U,N} \rangle$, respectively.

Using the definition for the variance of a binomial distribution, the standard deviation, σ_E, for the estimated rate was then used to determine a 95% confidence interval (*CI*), using the relationship

$$95\%CI \approx \lambda_E \pm 2\sigma_E = \lambda_E \pm 2\sqrt{m p_E (1 - p_E)} = [\lambda_{E,Lo}, \lambda_{E,Up}] \tag{24}$$

where $\lambda_{E,Up}$ and $\lambda_{E,Lo}$ are the upper and lower bounds for λ_E, respectively, and are defined as

$$\lambda_{E,Up} = \frac{\ln(1-p_{E,Up})}{-\tau_E}, \quad \lambda_{E,Lo} = \frac{\ln(1-p_{E,Lo})}{-\tau_E} \tag{25}$$

where

$$p_{E,Up} = \frac{\kappa_E + 2\sigma_E}{m}, \quad p_{E,Lo} = \frac{\kappa_E - 2\sigma_E}{m} \quad . \tag{26}$$

This allowed for an upper and lower bound of the standard error of the mean ($SEM_{E,Up}$ and $SEM_{E,Lo}$, respectively) to be calculated as

$$SEM_{E,Up} = \frac{(\lambda_{E,Up} - \lambda_E)}{1.96}, \quad SEM_{E,Lo} = \frac{(\lambda_E - \lambda_{E,Lo})}{1.96} \quad . \tag{27}$$

Implementing this statistical method provided extremely beneficial decreases in simulation time. It was found that for $\phi = 0$, each trajectory required about 30 minutes of simulation time to reach an $N = 3$ conformation, whereas for $\phi = 0.3$, each trajectory required about 10 hours (for the $R_c = R_r$ case) to reach $N = 3$. Therefore, in the latter case, to run $m = 200$ trajectories to completion would require about 2000 hours of simulation time (approximately 83 days). However, using this statistical method resulted in the same simulation to only require about 310 hours (13 days), and produced similar values with similar standard error. Therefore, this process was employed for determining the on-rate constants for the $N = 2$ and 3 conformations, as well as for all off-rate simulations, as it was these events that required the most simulation time. It should be noted that since the $N = 1$ and $N = 0$ on-rate constants had a 100% success rate (i.e. $\kappa_{N=0} = \kappa_{N=1} = m$), the mean and *SEM* could simply be calculated directly from the data.

RESULTS & DISCUSSION

In general, the process of reversible association can be broken down into three main steps: translational diffusion of the reactants to close proximity, followed by stereospecific binding, and, lastly, dissociation. Each of these steps was examined for reactants in the presence of crowding, and translational diffusion shall be discussed first.

Crowding reduces effective translational diffusivity

By monitoring a test molecule's mean squared displacement over an 80 nanosecond interval, its effective translational diffusion coefficient ($\overline{D}_T$) could be calculated as a function of time for different volume fractions and varying sizes of crowders. Figure 6a, below, shows that at a volume fraction of 0.3, the apparent diffusivity of the test molecule decreases relative to a non-crowded environment ($\phi = 0$), and the effect is only slightly stronger as the size of the crowding molecule decreases relative to the test molecule. It should be noted that the gradual drop in the effective diffusivity observed in Figure 6a, below, is due to the gradually increasing number of collisions between the test molecule and its neighboring molecules at short time scales.

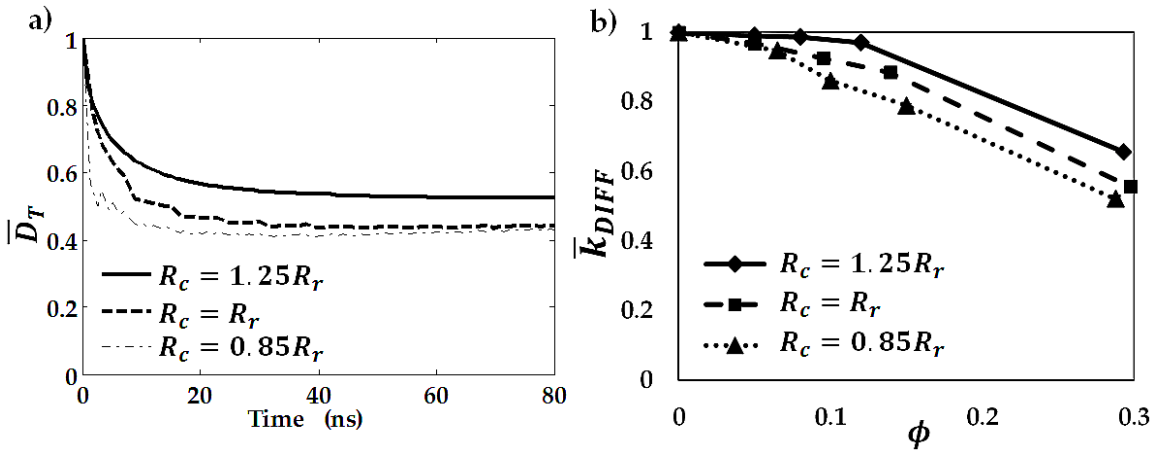

Figure 6. a) *Effective diffusivity of reactants as a function of volume fraction (ϕ), where* $\overline{D}_T = D_T\big|_{\phi=0.3} / D_T\big|_{\phi=0}$. ***b)*** *Reactant rates of arrival from a center-to-center separation distance of 9nm to 4.2nm, where* $\overline{k}_{DIFF} = k_{DIFF}\,|_{\phi} / k_{DIFF}\,|_{\phi=0}$.

The drop in diffusivity is also evident by the decrease in the normalized rates of arrival ($\overline{k}_{DIFF}$, as in Figure 4 in the Methods section, above) from the far-field regime to the near-field regime, as shown in Figure 6b. For higher volume fractions, the steric repulsion from the surrounding crowders hinders the overall mobility of the reactants, limiting their rates of arrival to the near-field regime.

Intuitively, the addition of macromolecules into the system should decrease the rate of arrival between two test molecules, as it is not hard to imagine that at higher volume fractions, the number of collisions between molecules increases, thus limiting the number of possible random walks each molecule can experience. Additionally, it can be seen that the fold drop in the effective diffusion coefficient is proportional to the fold decrease in the diffusion-limited rates of arrival when comparing Figure 6a to Figure 6b. In general, these findings are consistent with trends reported in previous

Brownian Dynamics simulations of crowding effects on diffusion (Wieczorek & Zielenkiewicz, 2008; Kim & Yethiraj, 2009). This proportionality also agrees with the Smoluchowski equation for diffusion-limited rates of equal sized spheres, which states that the diffusion-limited rate of arrival depends linearly on the effective diffusion coefficient (Smoluchowski, 1971).

Upon translationally diffusing to close proximity, the second step in the reversible association process is stereospecific binding.

Effects of crowding on association rates depend on stereospecificity

Due to the findings of Wieczorek and Zielenkiewicz (Wieczorek & Zielenkiewicz, 2008), and Kim and Yethiraj (Kim & Yethiraj, 2009) (as discussed in Chapter 1), it was hypothesized that there are important details in the stereospecificity of a reaction, as defined by Northrup and Erickson (Northrup & Erickson, 1992), that make it a key determinant of the reaction's sensitivity to crowding. Through simulating the association rates of stereospecific reactants (as described in the Methods section, above), the effects of crowding on association rates were found to be sensitive to two main parameters: the fraction of volume occupied by the crowding molecules, and the degree of stereospecificity required for the reactants to undergo a reaction. Observing Figure 7 below, it is evident that there is a dual effect on the association rate constants depending on the stereospecificity (N) of the reaction. At highest volume fractions (ϕ = 0.3), diffusion-limited (N = 0) reactions had a ~1.3-fold decrease in on-rate constant for

crowding molecules 1.25 times larger than reactants, and a ~2-fold decrease for equal-sized and smaller crowding molecules. On the other hand, for more stereospecific reactions (the $N = 2$ and $N = 3$ cases), and at the same volume fraction ($\phi = 0.3$), there was a two-to-threefold *increase* on the association rate constants, with minor variations for the different crowding molecule sizes (see Table A1 in Appendix for actual values).

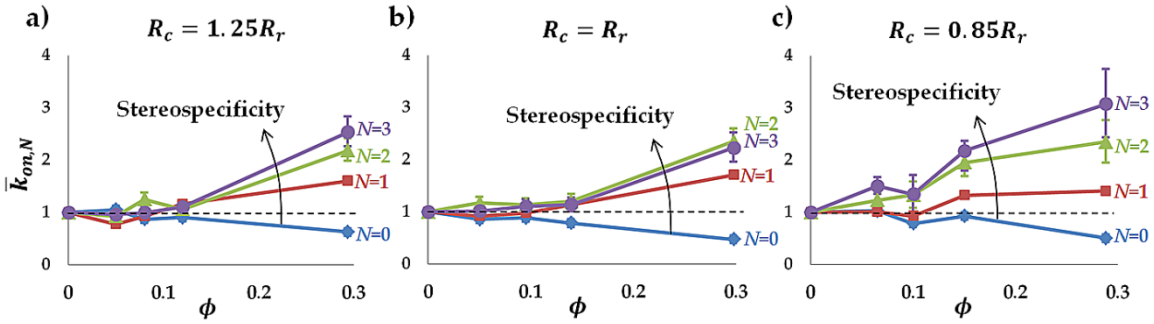

Figure 7. *Relative on-rate constants for varying crowder volume fractions (ϕ), and stereospecificity (N), where* $\bar{k}_{on,N} = k_{on,N}|_{\phi} / k_{on,N}|_{\phi=0}$. *Varying degrees of stereospecificity (N = 0-3) were investigated for crowding molecules being* ***a)*** *larger than,* ***b)*** *equal to, and* ***c)*** *smaller than the reactant molecules. Error bars are the standard error of the mean (SEM) as defined in the Data Analysis section.*

Essentially, the degree of stereospecificity is the determining factor as to how crowding affects the overall association rates: low stereospecificity, such as the diffusion-limited ($N = 0$) case, results in a *decrease* in the association rate with increasing volume fraction of crowding molecules, whereas a higher degree of relative rotational requirements (especially $N = 2$ and $N = 3$) results in an *increase* in association rate constant.

As discussed in Chapter 1, Kim and Yethiraj (2009) presented a model in which reactions that had low probabilities of occurring (per encounter), showed an increase in

association rates with higher volume fractions, whereas high-probabilistic reactions (such as the diffusion-limited case) had decreased association rates at the same volume fraction (Kim & Yethiraj, 2009). Although their model lacks important details pertaining to the conditional probability of stereospecific reactants undergoing a reaction (Qin *et al.*, 2012), they predicted the same trend presented here for similar conditions. Additionally, the computational model proposed by Wieczorek and Zielenkiewicz (discussed in Chapter 1) produced comparable results to those shown in this work. Their hen egg lysozyme/HyHEL-5 antibody model describes a particular case of a stereospecific association rate being enhanced due to crowding, whereas their non-stereospecific model showed a decrease in association rates, each of comparable magnitude to the fold-changes presented here (Wieczorek & Zielenkiewicz, 2008). However, the generality of the model in this work enables a wider variety of comparisons to experimental systems to be made, as compared to the limited predictions capable of Wieczorek and Zielenkiewicz's model (pertaining only to the particular case of the hen egg lysozyme/HyHEL-5 antibody system).

As discussed in Chapter 1, both the Wieczorek and Zielenkiewicz group and the Kim and Yethiraj group attributed their increases in association rates to a "caging" effect induced by the crowding molecules, keeping the reactants in close proximity for longer durations of time, allowing them more opportunities to react (Wieczorek & Zielenkiewicz, 2008; Kim & Yethiraj, 2009). It was hypothesized that, although neither group explicitly reported it, the "caging" effect they were referring to was in fact the

depletion forces theoretically predicted to be present in crowded environments by Asakura and Oosawa (Oosawa, 1954; Asakura & Oosawa, 1958). Thus, even though neither group had done so, it seemed that capturing the presence of depletion forces in the model presented here was necessary for explaining the observed increases of stereospecific association rate constants in crowded solutions.

Capturing the energetic landscape of a crowded environment

Quantifying the apparent energetic landscape, as experienced by reactant pairs in crowded environments (due to crowder-induced depletion effects, as described by Asakura and Oosawa (Oosawa, 1954; Asakura & Oosawa, 1958)), was a vital component for describing how their reaction kinetics are altered due to crowding. Thus, the apparent free energy due to depletion forces (ΔG_{DEP}) between two reactants, as a function of the radial separation distance (r) between them was computed (see Appendix) for the highest volume fraction investigated here (ϕ = 0.3), and is shown in Figure 8, below. For higher volume fractions, it is evident that the apparent interaction energy due to depletion forces is more negative when the pair of molecules approach one another (i.e. it is more favorable to be closer together, as predicted by Oosawa and Asakura (Oosawa, 1954; Asakura & Oosawa, 1958)). This effect is not sensitive to the range of sizes of crowding molecules studied, which agrees well with the minimal changes in association rates between crowding scenarios (i.e. comparing Figures 7a, 7b, and 7c).

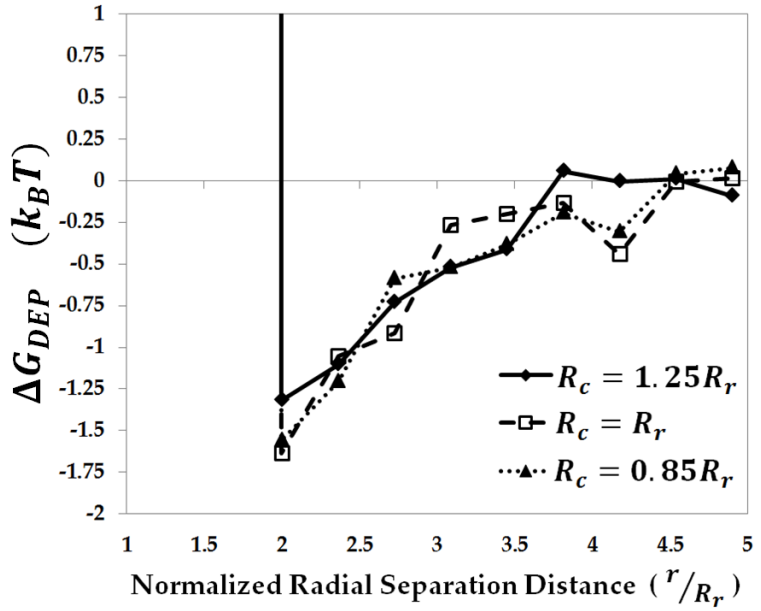

Figure 8. *Induced free energy due to depletion forces (ΔG_{DEP}), (as a function of radial separation distance between reactant pairs, r) on reactants in close proximity due to crowding (for $\phi = 0.3$). Depletion forces act on molecular pairs less than L_{crit} apart from one another, biasing their translational diffusion toward one another. Due to the hard-sphere assumption, there is infinite repulsion upon the collision of reactant surfaces (i.e. when $r = 2R_r$).*

Although quantifying the energetic effects of depletion forces was a good first step in explaining the changes association rate constants, it was still unclear exactly how more stereospecific reactants were benefitting from this additional free energy while in close proximity more so than non-specific reactions. Thus, further investigation was required.

Depletion forces prolong encounters to drive more efficient transitions from partially bounded states ($N = 0$, $N = 1$) to more completely bounded states ($N = 2$, $N = 3$)

In the model, an encounter was defined to begin when reactant surfaces came within 2Å of one another, regardless of rotational configuration. Each subsequent

encounter was not counted until the reactants had diffused away to some critical, center-to-center, distance, and then back to 2Å, edge-to-edge, ensuring that an encounter was not simply defined as a re-collision event via stochastic motion of reactants in close proximity. This critical, center-to-center distance was defined as the minimum required amount of separation between reactants such that one crowding sphere's centroid could be placed collinearly with both reactant centroids. Therefore, the critical distance varied with the dimensions of the crowding molecule, as

$$L_{crit} = 2(R_r + R_c) \quad . \tag{28}$$

It is interesting to note that the interaction potential described in Figure 8 approaches zero near the critical length for each crowder size (i.e. when $r \to L_{crit}$), as initially predicted by Asakura and Oosawa (Oosawa, 1954; Asakura & Oosawa, 1958).

Given that the overall on-rate constants increase with increasing volume fractions for stereospecific bonds (i.e. when N = 2 or N = 3) while the overall far-field diffusion of the reactants is inhibited, suggests that there is a higher degree of efficiency during each reactant encounter that not only negates, but overcompensates for the negative effects of effectively slower translational diffusion in a crowded environment. Consequently, the overall average time spent by the reactants diffusing prior to achieving a highly stereospecific bond actually *decreases* with the addition of crowding molecules, providing a net increase in the association reaction rate, as seen in Figure 7 (see, also, Table A1 in Appendix).

Figure 9, below, shows that at higher volume fractions, fewer encounters are required for 100% of the trajectories to reach an $N = 3$ conformation.

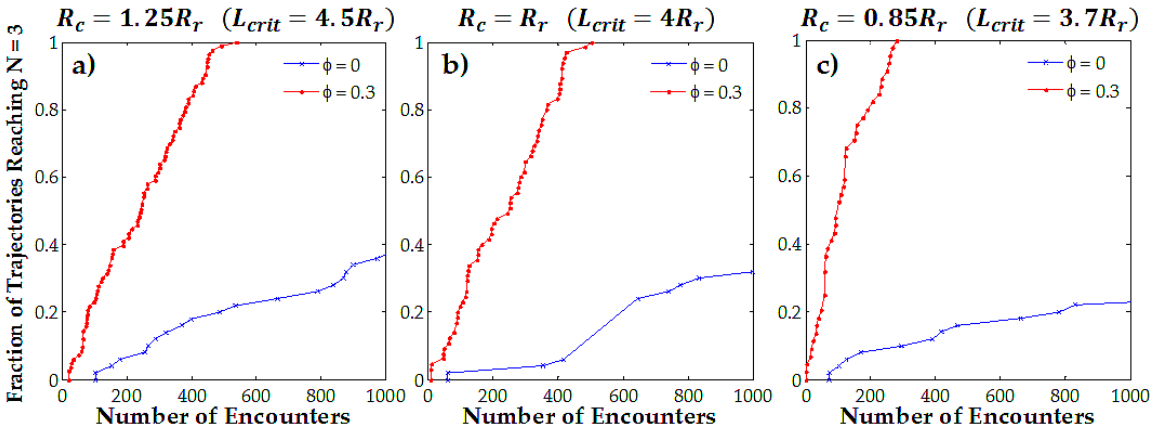

Figure 9. *Cumulative distribution function of the number of encounters at low ($\phi = 0$) and high ($\phi = 0.3$) volume fractions prior to reaching an $N = 3$ conformation for crowding molecules* ***a)*** *larger than,* ***b)*** *equal to, and* ***c)*** *smaller than the reactant molecules.*

It was found that the presence of crowding molecules increases the efficiency of each encounter by increasing the probability of forming a complete bond at each encounter. Once the reactants diffuse to within close proximity (< L_{crit}), depletion forces originating from steric repulsions from crowders surrounding the edges of a reactant pair (Oosawa, 1954; Asakura & Oosawa, 1958) act as an entropic spring, biasing the reactants' translational diffusion toward one another. These depletion forces will drive the reactants to an overall closer separation distance during an encounter, enabling greater interactions between each respective reactive zone (see Table A4 in Appendix), thus increasing the probability that the proper orientational configuration between reactants will be achieved during the encounter.

Additionally, depletion forces will prolong the duration of encounters, allowing even more rotational configurations to be explored per encounter (see Table A6 in Appendix). This "caging effect", or entrapment of the reactants, coupled with the average smaller separation distance during an encounter, decreases the number of encounters needed prior to reaching the proper relative orientation to react (Figure 9). Thus, the combination of these two consequences of depletion forces acting on reactants in close proximity drives more efficient encounters. This agrees well with arguments made by Northup and Erickson, where they discussed that, even in the absence of crowders, two reactants have enough time to explore multiple rotational configurations during a single encounter, explaining the ~400-fold difference between their simulated association rates, and rates predicted purely by geometric parameters (Northrup & Erickson, 1992).

From the simulation, it was possible to determine which step in stereospecific association was rate-limiting, and examine how this step was enhanced in the presence of crowders. This was accomplished by monitoring the number of times a given conformation was achieved relative to another conformation in a single trajectory of reactant pairs. For example, the number of times an $N = 2$ conformation was achieved by the reactants prior to reaching an $N = 3$ conformation (in the same trajectory) was denoted as the conformation ratio ($N = 3$):($N = 2$), as in Table 1, below.

Table 1. *Efficiency of transitioning to higher degrees of stereospecific conformations.*

Conformation Ratio	ϕ		**Fold Increase**
	0	**0.3**	
(N = 1):(N = 0)	0.0854	0.2267	2.655
(N = 2):(N = 1)	0.0041	0.0141	3.439
(N = 3):(N = 2)	0.6747	0.9103	1.349

Table 1 shows that, for increasing volume fractions, the probability that reactants in an N = 1 conformation eventually lead to an N = 2 conformation (i.e. (N = 2):(N = 1)) increases by over 3-fold. If reactants are in an N = 1 conformation, their relative rotational orientations are much more correlated than if they are not in any conformation as defined here, and the longer durations of time prior to diffusing apart allow more opportunities for an N = 2 conformation to be achieved. Since achieving the N = 2 conformation is the rate-limiting step in forming a complete (N = 3) bond (see Appendix), an acceleration of this step most strongly contributes to the overall increase in the association rates.

After translationally diffusing to close proximity and undergoing stereospecific binding, the final step in reversible association is the unbinding of the reactants, and its sensitivity to crowding is discussed below.

Dissociation is weakly slowed by crowding because of rotational correlation during bond breakage

The decrease of off-rate constants with increasing volume fraction observed in Figure 10 and Table 2 can also be explained by the depletion forces due to crowding. The

additional free energy imposed on the reactants while in close proximity makes it more difficult for them to separate, as shown by the overall decreasing trends in the off-rates. The steric repulsion due to crowding molecules (depletion forces) surrounding bound reactants will limit their translational escape routes, forcing them to stay together, increasing the time spent in the bound state and decreasing their off-rate constants.

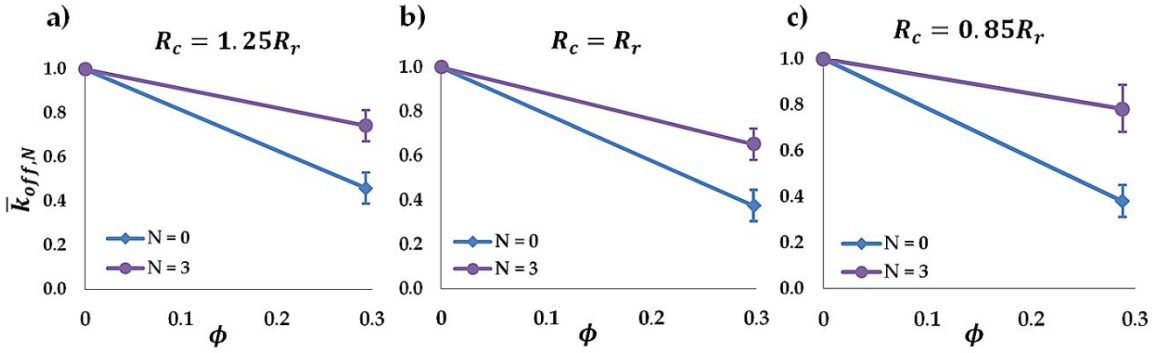

Figure 10. *Normalized off-rate constants for varying crowder volume fractions (ϕ) and for crowding molecules* ***a)*** *larger than,* ***b)*** *equal, and* ***c)*** *smaller than reactant molecules, where* $\bar{k}_{off,N} = k_{off,N}|_{\phi} / k_{off,N}|_{\phi=0}$ *. The dissociation of the reactants starting from the N = 0 and N = 3 conformations were investigated (*Insufficient data). Error bars are the standard error of the mean (SEM) as defined in the Data Analysis section.*

Intuitively, one might expect that the fold-decrease in off-rate should be the same as the fold increase in the on-rate for identical crowding conditions. However, observing Figures 7 and 10, above, it is clear that dissociation is more weakly affected by crowding than association. This can be explained in terms of rotational correlation. In general, if the reactants' diffusive step results in a positive change in energy (i.e. going from a higher conformation (N = 3 or N = 2) to a lower (N = 1 or 0) conformation), it is likely that they immediately reform whatever conformation they were previously in,

regardless of whether or not depletion effects are present. This is because the stochastic nature of their diffusion makes it as equally probable that they will step back to where they previously were, as it is that they will step further apart. Therefore, in general, the dissociation of reactants is a *translational* diffusion-driven process, rather than rotational. However, since the *association* of the reactants relies heavily on their ability to rotationally explore multiple relative orientations (as discussed above), there is much to be benefitted from the presence of depletion forces, but, since there is no opposite of this effect for *dissociation* (that is, the reactants do not dissociate based on rotational exploration, regardless of the crowding environment), there is less of an effect of crowding on dissociation. This is also supported by the fact that the diffusion-limited dissociation (a purely translationally diffusive process by definition) decreases for increasing volume fractions and does not depend strongly on stereospecificity, as seen in Figure 10, above.

Another interesting observation is that dissociation of the $N = 0$ conformation is more strongly influenced by crowders than the $N = 3$ case. While in the $N = 3$ conformation, a significant amount of the rotational and translational degrees of freedom have been taken away from the reactants due to the strength of the bond between them. This is also supported by the ~$13k_BT$ entropic penalty imposed on the reactants due to being in the bound state (Table 2, below). Therefore, the presence of crowders does not greatly contribute to the loss of translational and rotational freedom of the reactants, since the majority of it has already been taken away. However, for the

$N = 0$ case, any loss in rotational and translational freedom of the reactants is *strictly* due to the presence of crowders, since there is no bond energy associated with this conformation. Therefore, crowding more strongly affects dissociation of the unbound reactants than for the bound reactants.

Depletion forces due to crowding increase reactant affinity

Since the forward and reverse reaction rate constants were both simulated, the changes in equilibrium constant and standard Gibbs free energy as functions of crowder volume fraction and reactant stereospecificity could be calculated. When observing Table 2, it is interesting to note the decreases in the entropic penalty and standard Gibbs free energy with increasing crowder volume fractions. By the reactants being separated by a distance less than L_{crit}, the local available volume to the crowders increases, thus increasing their entropy and providing a paradoxical, favorable increase in entropy to the system (Marenduzzo *et al.*, 2006). Therefore, since it is more favorable for the reactants to be in contact when in close proximity, their overall affinity increases, which manifests itself in the simulation as a decrease in $k_{off,N}$, and, consequently, a more negative ΔG_N^o. Since the intrinsic bond strength ($\Delta G_{B,N}^o$) remains roughly constant regardless of crowding, the increased affinity (i.e. decrease in ΔG_N^o) must result in a drop in the entropic penalty felt by the reactants due to binding ($\Delta G_{S,N}^o$), per Eq. 20. Therefore, for stereospecific ($N = 3$) bonds, the overall effects of crowding result in a

~3.5-fold increase in the equilibrium constant, $K_{eq,3}$ (where $K_{eq,3} = k_{on,3} / k_{off,3}$), as seen in Table 2, below. (See Table A5 in the Appendix for the diffusion-limited case).

Table 2. *Numerical values for simulated N=3 off-rate constants and thermodynamic parameters.*

Crowding Molecules	ϕ	$k_{off,3}$ (ms^{-1})	$K_{eq,3}$ M^{-1}	ΔG_3^o (k_BT)	$\Delta G_{B,3}^o$ (k_BT)	$\Delta G_{S,3}^o$ (k_BT)
	0	20.02	108.8	-4.69	-18.50	13.81
$R_c = 1.25R_r$	0.29	17.15	370.0	-5.77	-18.47	12.69
$R_c = R_r$	0.30	13.07	370.9	-5.92	-18.42	12.51
$R_c = 0.85R_r$	0.29	15.67	427.5	-6.06	-18.23	12.17

It is interesting to note that the magnitude of the drop in potential energy due to the added interaction energy from depletion effects (represented in Figure 8) agrees well with the drop in overall Gibbs free energy in Table 2 for each of the crowding situations (excluding the off-rates for smallest crowding molecules due to a lack of data). Additionally, the amount of energy due to depletion forces (~1k_BT) also agrees well with the ~e-fold decrease in the off-rate for the diffusion-limited case ($k_{off,0}$) observed in Figure 10 and Table A5, as well as with the experimental data presented by Yodh *et al*. as discussed above in Chapter 1 (Yodh *et al*., 2001).

Visual Summary of Crowding-mediated Effects on Reversible Association

Given that the process of reversible association was examined in three main steps, it is simple to summarize the overall effects of crowding on each step, as shown below, in Figure 11.

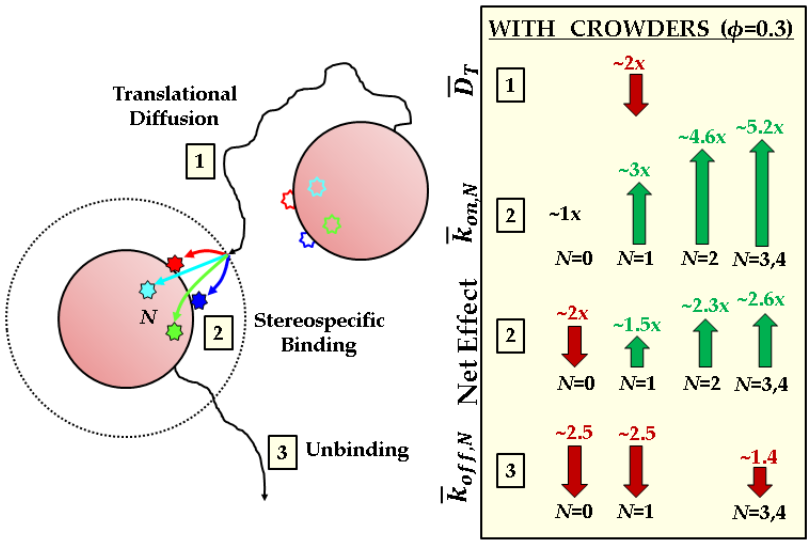

Figure 11. *Visual summary of effects of crowding for ϕ=0.3 on each step in the process of reversible association.*

Observing Figure 11, above, it is easy to see that even though the translational diffusivity of the reactants in crowded environments decreased by about 2-fold, the net effect of crowding after stereospecific binding of the reactants depends strongly on the stereospecificity, as discussed above. Figure 11 also shows that the dissociation of the reactants is only weakly hindered by crowding, but also depends on the strength of the bond between the reactants, as also discussed in the preceding sections (see Table 2, above, and Table A5 in the Appendix, below, for all numerical values).

Thermodynamic Discussion

As stated in Chapter 1, Minton *et al*. predicted that, due to their assumption that the thermodynamic equilibrium constants of reactants in crowded media depend on the

"excluded volume" of the system after the addition of crowders, the equilibrium constants for reactants in the system will increase by *orders of magnitude* (Minton, 1983; Minton & Wilf, 1981; Zhou *et al.*, 2008; Hall & Minton, 2003; Minton, 2006; Ellis & Minton, 2003). However, the model presented in this work predicts very modest changes in equilibrium constants with the addition of crowders (K_{eq} increases by ~3.5-fold). As discussed in the Volume Fraction section above, due to the *diffusion* of the molecules in the system, there is some probability that every molecule will explore *every* unit of space in the domain, provided a long enough duration of time. Therefore, it is argued that there is *not any* excluded volume in the system. This lack of consideration of transport theory is a fundamental error in the key assumption of "excluded volume", of which Minton *et al.* based the majority of their predictions.

Consequences of Adding Crowders to Solutions *in vitro*

First, it is important to consider that if the crowding molecules become sufficiently small relative to the reactants, they essentially act as solvent molecules from the reactant's perspective, and will behave as in the $\phi = 0$ case, although with a different (likely higher) viscosity than the solvent (e.g. water). Therefore, there is some lower limit on the size of crowding molecules that will cause the effects discussed in this work. Moreover, the opposite case can also be argued, which is that crowders much larger than the molecules of interest diffuse much slower and are less influential, and, therefore, also cannot be regarded as crowding molecules. In this case, there may in fact

be excluded volume due to stationary/slowly diffusing organelles (e.g. mitochondria, nuclei). It is important to only consider crowding to occur where crowding molecules and reactants are similar in dimension.

Secondly, the model presented here suggests that for high volume fractions of crowding molecules, at most, a threefold increase and a twofold decrease in the association rates and dissociation rates, respectively, can be expected for similar experimental conditions (i.e. roughly a 3.5-fold increase in K_{eq} for N = 3 stereospecific associations). Energetically, this corresponds to only a $\Delta\Delta G^o \cong -k_B T \ln(3.5) = -1.3 k_B T$ energy change, roughly equivalent to a hydrogen bond. Therefore, the addition of macromolecules to the solvent of an *in vitro* experiment are not predicted to produce large, order-of-magnitude changes in the reaction kinetics, as recently reported experimentally by Wieczorek *et al*. (Wieczorek *et al*., 2013). If such effects are observed, they are more likely due to a thermodynamic reordering of the energetic state of the solvent through interactions between the macromolecules and water molecules (Winzor & Wills, 2006), rather than due to the enhanced efficiency of encounters due to depletion forces, as discussed in this model. With that, it is recommended that the addition of macromolecules to an *in vitro* experiment, in attempts to recreate the intracellular environment, should not be done without sufficient knowledge of the macromolecules' precise effects on the state of the solvent. A more reliable correction might be to avoid the addition of crowding molecules to experiments *in vitro* altogether, and simply adjust

the rate constants by the fold changes presented in this work based on the size of reactants, relative size of the crowding agents, and the apparent volume fraction of the *in vivo* environment of interest.

Relevance to evolution in cellular biology

The results of this work suggest that crowders do not have a strong effect on the overall reaction kinetics and thermodynamics of biomolecules. Therefore, cytoplasmic reactions are also predicted to be unaffected by fluctuations in local microenvironments, suggesting that overall cellular function has evolved to be insensitive to changes in intracellular crowding composition. That is, there is little evolutionary pressure for biomolecules to evolve to some optimal stereospecificity given the extent of crowding in their environment, since there are only small favorable energetic contributions in doing so, as shown by this model.

CONCLUSIONS

Changes in overall biochemical reaction kinetics in the presence of macromolecular crowding agents were investigated with a computational model using Brownian dynamics. It was determined that depletion forces (due to crowding) provide a favorable energetic contribution (~1k_BT) to reactants in close proximity, effectively increasing the overall reactant affinity. However, decreased diffusivity in the far-field

inhibits reactant encounters, and by itself tends to reduce the association equilibrium (affinity) constant. Therefore, the degree of stereospecificity of the reactants is the determining factor as to how the reactants are affected by the depletion forces due to crowding. Diffusion-limited reactions in crowded solutions do not significantly benefit from the increased affinity once in close proximity, disabling them from the ability to overcompensate for the inhibited long-range diffusivity, thereby decreasing their association rate constants. However, more stereospecific reactions are able to explore more relative rotational conformations once in close proximity, as well as being forced closer together in crowded environments than in a buffer solution (both due to depletion forces), which decreases the amount of time spent diffusing prior to completing a bond, effectively increasing their association rate. Additionally, since bound reactants remain rotationally correlated during separation, their dissociation is a translational diffusion-driven process. Therefore, depletion forces can only hinder the bound reactants' ability to dissociate (i.e. decreases their dissociation rates), and their dissociation depends weakly on stereospecificity.

However, in the most extreme cases investigated in this model, the combination of the effects of crowding on association and dissociation only result in about a 3.5-fold increase in the equilibrium constant for highly stereospecific reactions. Therefore, when studying reactions *in vitro*, the addition of crowding agents to the solution is not recommended, as the energetic reordering of the solvent is, at present, unpredictable for different crowding reagents. Rather, reactions should be studied in buffer solutions,

with a final adjustment of the equilibrium constant based on the fold changes presented here, depending on the stereospecificity of the reaction, relative molecular sizes, and the *in vivo* volume fraction of interest. In the future, it will be important to test the model predictions experimentally, and to critically assess the contributions of so-called "crowding" agents to the solvent thermodynamics.

CHAPTER 3

FURTHER REMARKS

Bodystorming

Complementing the design of the computational model presented here, a novel and modern approach to characterizing the effects of macromolecular crowding took the form of a human movement and interaction study. Members of the Black Label Movement, a performing arts and dance theater based in Minneapolis, MN, were asked to participate in a qualitative experiment, of which the combinations of dance and diffusion theory, coupled with direct feedback through verbal communication, provided new, insightful perspectives of the computational model— a useful brainstorming technique known as "bodystorming" (Flink & Odde, 2012).

Each participant was given a set of rules to follow, such that their collective movement would loosely demonstrate a system of molecules undergoing Brownian motion in a confined domain. Dancers were asked to take translational steps with each half-beat of the rhythm of a song, as well as to rotate roughly 45 degrees with each step. They were also confined to a square domain on the dance floor, of which "reflective boundary conditions" were implemented, similar to the computational model design. Next, two people of interest were chosen as the "reactants" of the system surrounded by various amounts of other non-reactive dancers (i.e. crowders). The time it took for the

two dancers of interest to collide (with no orientational constraints) was calculated for the cases of having 4 people in the domain (2 "reactants" and 2 "crowders"), as well as 9 people, total (2 "reactants" and 7 "crowders"). The reciprocal of this time was said to be the "on-rate constant" for this "diffusion-limited association reaction".

The results of this qualitative experiment agree well with predictions made by the computational model. The "on-rate constant" for the case of having more people on the dance floor resulted in a statistically significantly ($p < 0.02$) decrease relative to the less crowded dance floor. This result agrees with the overall decreasing trend for the diffusion-limited, Smoluchowski (i.e. $N = 0$ case) scenario predicted by the computational model presented here. Additionally, the visualization of the active system, coupled with direct verbal feedback from participants, provided a uniquely beneficial and productive environment for developing new concepts to be implemented in the computational model.

Future Work

In the immediate future, certain components of the results of this model will be addressed. For one thing, a more complete collection of dissociation simulation data will be necessary, as Table 2 and Figure 10 are lacking values.

More generally, it is clear that the model presented here is quite simplistic with regards to many of the assumptions made. For one thing, the hard-sphere interaction

assumption is a good approximation (Hall & A. P. Minton 2003) for this type of stochastic simulation, however, some would argue that there should be soft interactions between colliding molecules (Kim *et al.*, 2010). Conservation of energy was also not accounted for at each collision of molecules, which would dictate the velocity of the molecules after each collision (however, greatly increasing the computational cost of the simulation). Additionally, this model assumes no hydrodynamic interactions between the molecules and the solvent. The use of hydrodynamic interactions could be introduced into the model to further mimic an *in vivo* environment (Długosz & Trylska 2011; Ermak & McCammon 1978; Ando & Skolnick 2010), and would be an interesting addition. By including hydrodynamic interactions, further effects due to crowding could be investigated and compared to those without hydrodynamic interactions, providing an assessment of the contributions made from these interactions. Provided the long-term continuation of this model in the future, all of these additions would be a contributable asset to quantifying more of the details in the effects of crowding in the cytoplasm.

Certain components of this model presented many challenges when attempting to expand on the parameter space it explores. As stated in Chapter 2, the simulation run-time became extremely cumbersome, especially when investigating the dissociation rates, or large numbers of crowding molecules. Therefore, experimenting with other assumptions embedded in the model was difficult. Provided more time and computational resources, some components of the model would be tested. For one

thing, the square-well potential used in this model is an artifact of reproducing work originally done by Northrup and Erickson, as this was the potential well they had assumed for their protein-protein association model (Northrup & Erickson 1992). The use of a harmonic potential might be a more realistic model of the spring-like characteristics generally accepted for the type of bimolecular bond being modeled here. Each of the four zones would have its own harmonic potential such that each time another zone associates with its partner zone, another harmonic potential would contribute to the overall strength of the bond (like adding springs in parallel). Modeling the potential energy in this manner would not only be more realistic, but would provide insight as to how valid of an approximation the square-well potential used here actually is. Additionally, a Lennard-Jones type of potential could be tested for similar purposes.

Aside from possible additions to the model, an interesting component to consider is the model's potential to estimate the extent of stereospecificity from the association rate constant. For biomolecules with values of k_{on} = 1-10$\mu M^{-1}s^{-1}$ in the absence of crowding molecules, this corresponds to an N = 3 reaction in this model (as well as Northrup and Erickson's model (Northrup & Erickson 1992)). However, in the presence of crowding (i.e. in the cytoplasm), measured on-rate constants can be compared to those presented in this work corresponding to the estimated volume fraction of the environment, and a degree of stereospecificity could be estimated for that reactant pair. This could be beneficial for estimating more specific characteristics of macromolecules in the cytoplasm, such as surface charge distribution or overall protein conformation.

Lastly, validating certain parts of this model through *in vitro* experiments would be extremely valuable. Recently, Dr. Xiang Cheng and his lab group in the Department of Chemical Engineering at the University of Minnesota have successfully created an experimental environment much like the simulation domain described in this work. They are able to image the diffusion of colloidal particles in a small, controlled environment with variable amounts of crowding molecules. Through Dr. Cheng's techniques, it is hoped that an experimental validation of certain components of this model could be performed. Certainly, a comparison between the inhibited diffusion of molecules in Dr. Cheng's crowding system could be made with those predicted in this model, assuming very similar characteristics of each domain are achievable. Although studying stereospecific reactions in Dr. Cheng's experimental setting would likely be much more challenging than studying pure diffusion, certain scenarios might be feasible. For one thing, the use of commercially available reactive reagents could be beneficial. Given macromolecules with similar reactive characteristics to those proposed in this work, an experimental correlation between these molecules in Dr. Cheng's system and those presented here would provide much enlightenment as to how the assumptions made in this model compare to those seen in *in vitro* systems.

Overall, it is hoped that the generality and robustness of the model presented in this work will provide new insight to those studying biochemical reactions *in vitro*. Through answering some of the previously unanswered questions regarding how crowding affects biochemical reaction kinetics and thermodynamics in the cytoplasm,

researchers and scientists studying these reactions should now have a better understanding of the compatibility between observations made in *in vitro* systems and those of the intracellular domain, as well as elucidating how, if desired, the effects of crowding should be handled when modeling *in vivo* systems. Through this deeper understanding of the physical mechanisms and thermodynamics in crowded, intracellular environments, those studying these systems can conduct valuable research with a higher degree of confidence that the effects of macromolecular crowding are well-accounted for.

REFERENCES

Ando, T. & Skolnick, J., 2010. Crowding and hydrodynamic interactions likely dominate in vivo macromolecular motion. *Proceedings of the National Academy of Sciences of the United States of America*, 107(43), pp.18457–62. Available at: http://www.pubmedcentral.nih.gov/articlerender.fcgi?artid=2973006&tool=pmcentrez&rendertype=abstract [Accessed May 24, 2013].

Asakura, S. & Oosawa, F., 1958. Interactions between Particles Suspended in Solutions of Macromolecules. *Journal of Polymer Science*, 33, pp.183–192.

Banks, D.S. & Fradin, C., 2005. Anomalous diffusion of proteins due to molecular crowding. *Biophysical journal*, 89(5), pp.2960–71. Available at: http://www.pubmedcentral.nih.gov/articlerender.fcgi?artid=1366794&tool=pmcentrez&rendertype=abstract [Accessed May 22, 2013].

Długosz, M. & Trylska, J., 2011. Diffusion in crowded biological environments: applications of Brownian dynamics. *BMC biophysics*, 4(1), p.3. Available at: http://www.pubmedcentral.nih.gov/articlerender.fcgi?artid=3093676&tool=pmcentrez&rendertype=abstract [Accessed June 6, 2013].

Ellis, R J, 2001. Macromolecular crowding: an important but neglected aspect of the intracellular environment. *Current opinion in structural biology*, 11(1), pp.114–9. Available at: http://www.ncbi.nlm.nih.gov/pubmed/11179900.

Ellis, R John & Minton, A.P., 2003. Join the Crowd. *Nature*, 425, pp.27–28.

Ermak, D.L. & McCammon, J. a., 1978. Brownian dynamics with hydrodynamic interactions. *The Journal of Chemical Physics*, 69(4), p.1352. Available at: http://link.aip.org/link/JCPSA6/v69/i4/p1352/s1&Agg=doi [Accessed May 24, 2013].

Flink, C. & Odde, D.J., 2012. Science + dance = bodystorming. *Trends in cell biology*, 22(12), pp.613–6. Available at: http://www.ncbi.nlm.nih.gov/pubmed/23122551 [Accessed August 5, 2013].

Frederick, K.B., Sept, D. & De La Cruz, E.M., 2008. Effects of solution crowding on actin polymerization reveal the energetic basis for nucleotide-dependent filament stability. *Journal of molecular biology*, 378(3), pp.540–50. Available at: http://www.pubmedcentral.nih.gov/articlerender.fcgi?artid=2424216&tool=pmcentrez&rendertype=abstract [Accessed June 6, 2013].

Fulton, A.B., 1982. How Crowded is the Cytoplasm? *Cell*, 30, pp.345–347.

Hall, D. & Minton, A.P., 2003. Macromolecular crowding: qualitative and semiquantitative successes, quantitative challenges. *Biochimica et Biophysica Acta (BBA) - Proteins and Proteomics*, 1649(2), pp.127–139. Available at: http://linkinghub.elsevier.com/retrieve/pii/S1570963903001675 [Accessed June 3, 2013].

Howard, J., 2001. *Mechanics of Motor Proteins and the Cytoskeleton*, Sinauer Associates, Inc.

Kim, J.S. & Yethiraj, A., 2010. Crowding effects on association reactions at membranes. *Biophysical journal*, 98(6), pp.951–8. Available at: http://www.pubmedcentral.nih.gov/articlerender.fcgi?artid=2849078&tool=pmcentrez&rendertype=abstract [Accessed June 6, 2013].

Kim, J.S. & Yethiraj, A., 2009. Effect of macromolecular crowding on reaction rates: a computational and theoretical study. *Biophysical journal*, 96(4), pp.1333–40. Available at: http://www.pubmedcentral.nih.gov/articlerender.fcgi?artid=2717233&tool=pmcentrez&rendertype=abstract [Accessed June 6, 2013].

Kim, Y.C., Best, R.B. & Mittal, J., 2010. Macromolecular crowding effects on protein-protein binding affinity and specificity. *The Journal of chemical physics*, 133(20), p.205101. Available at: http://www.ncbi.nlm.nih.gov/pubmed/21133453 [Accessed August 19, 2013].

Kozer, N. & Schreiber, G., 2004. Effect of crowding on protein-protein association rates: fundamental differences between low and high mass crowding agents. *Journal of molecular biology*, 336(3), pp.763–74. Available at: http://www.ncbi.nlm.nih.gov/pubmed/15095986 [Accessed June 3, 2013].

Lindner, R. & Ralston, G., 1995. Effects of dextran on the self-association of human spectrin. *Biophysical chemistry*, 57(1), pp.15–25. Available at: http://www.ncbi.nlm.nih.gov/pubmed/8534835.

Marenduzzo, D., Finan, K. & Cook, P.R., 2006. The depletion attraction: an underappreciated force driving cellular organization. *The Journal of cell biology*, 175(5), pp.681–6. Available at: http://www.pubmedcentral.nih.gov/articlerender.fcgi?artid=2064666&tool=pmcentrez&rendertype=abstract [Accessed August 7, 2013].

Metropolis, N. & Ulam, S., 1949. The Monte Carlo Method. *Journal of the American Statistical Association*, 44(247), pp.335–341.

Minton, A., 1983. The effect of volume occupancy upon the thermodynamic activity of proteins: some biochemical consequences. *Molecular and cellular biochemistry*, 140, pp.119–140. Available at: http://link.springer.com/article/10.1007/BF00673707 [Accessed August 5, 2013].

Minton, A.P., 2006. How can biochemical reactions within cells differ from those in test tubes? *Journal of cell science*, 119(Pt 14), pp.2863–9. Available at: http://www.ncbi.nlm.nih.gov/pubmed/16825427 [Accessed May 25, 2013].

Minton, A.P., 1997. Influence of excluded volume upon macromolecular structure and associations in "crowded" media. *Current opinion in biotechnology*, 8(1), pp.65–9. Available at: http://www.ncbi.nlm.nih.gov/pubmed/9013656.

Minton, A.P., 2001. The Influence of Macromolecular Crowding and Macromolecular Confinement on Biochemical Reactions in Physiological Media. *The Journal of Biological Chemistry*, 276(14), pp.10577–10580.

Minton, A.P. & Wilf, J., 1981. Effect of macromolecular crowding upon the structure and function of an enzyme: glyceraldehyde-3-phosphate dehydrogenase. *Biochemistry*, 20(17), pp.4821–6. Available at: http://www.ncbi.nlm.nih.gov/pubmed/7295652.

Northrup, S.H. & Erickson, H.P., 1992. Kinetics of protein-protein association explained by Brownian dynamics computer simulation. *Proceedings of the National Academy of Sciences of the United States of America*, 89(8), pp.3338–42. Available at: http://www.pubmedcentral.nih.gov/articlerender.fcgi?artid=48862&tool=pmcentrez&rendertype=abstract.

Oosawa, F., 1954. On Interaction between Two Bodies Immersed in a Solution of Macromolecules. *The Journal of Chemical Physics*, 22(7), p.1255. Available at: http://link.aip.org/link/JCPSA6/v22/i7/p1255/s2&Agg=doi [Accessed July 30, 2013].

Phillip, Y. & Schreiber, G., 2013. Formation of protein complexes in crowded environments--from in vitro to in vivo. *FEBS letters*, 587(8), pp.1046–52. Available at: http://www.ncbi.nlm.nih.gov/pubmed/23337873 [Accessed August 5, 2013].

Qin, S., Cai, L. & Zhou, H.-X., 2012. A method for computing association rate constants of atomistically represented proteins under macromolecular crowding. *Physical*

biology, 9(6), p.066008. Available at: http://www.ncbi.nlm.nih.gov/pubmed/23197255 [Accessed August 16, 2013].

Smoluchowski, M. von, 1971. Study of Mathematical Theory for the Coagulation Kinetics of Colloidal Solutions.

Wieczorek, G. & Zielenkiewicz, P., 2008. Influence of macromolecular crowding on protein-protein association rates--a Brownian dynamics study. *Biophysical journal*, 95(11), pp.5030–6. Available at: http://www.pubmedcentral.nih.gov/articlerender.fcgi?artid=2586562&tool=pmcentrez&rendertype=abstract [Accessed June 6, 2013].

Wieczorek, M., Chaaban, S. & Brouhard, G.J., 2013. Macromolecular Crowding Pushes Catalyzed Microtubule Growth to Near the Theoretical Limit. *Cellular and Molecular Bioengineering*. Available at: http://link.springer.com/10.1007/s12195-013-0292-9 [Accessed August 11, 2013].

Winzor, D.J. & Wills, P.R., 2006. Molecular crowding effects of linear polymers in protein solutions. *Biophysical chemistry*, 119(2), pp.186–95. Available at: http://www.ncbi.nlm.nih.gov/pubmed/16129549 [Accessed August 19, 2013].

Yodh, a. G. et al., 2001. Entropically driven self-assembly and interaction in suspension. *Philosophical Transactions of the Royal Society A: Mathematical, Physical and Engineering Sciences*, 359(1782), pp.921–937. Available at: http://rsta.royalsocietypublishing.org/cgi/doi/10.1098/rsta.2000.0810 [Accessed August 10, 2013].

Zhou, H.-X., Rivas, G. & Minton, A.P., 2008. Macromolecular crowding and confinement: biochemical, biophysical, and potential physiological consequences. *Annual review of biophysics*, 37, pp.375–97. Available at: http://www.pubmedcentral.nih.gov/articlerender.fcgi?artid=2826134&tool=pmcentrez&rendertype=abstract [Accessed May 25, 2013].

Zimmerman, S.B. & Minton, A.P., 1993. Macromolecular Crowding: Biochemical, Biophysical, and Physiological Consequences. *Annual Review of Biophysics and Biomolecular Structure*, 22(June), pp.27–65.

CHAPTER 4

APPENDIX

Supporting Tables

Table A1. *On-rate constants for varying degrees of stereospecificity.*

Crowding Molecules	ϕ	$k_{on,0,1}$ $(nM^{-1}s^{-1})$		$k_{on,2,3}$ $(\mu M^{-1}s^{-1})$	
		N = 0	**N = 1**	**N = 2**	**N = 3**
	0	7.43	0.55	4.50	2.18
$R_c = 1.25R_r$	0.05	7.82	0.43	4.16	2.09
	0.08	6.48	0.51	5.62	2.16
	0.12	6.72	0.64	4.77	2.40
	0.29	4.67	0.88	9.81	5.51
$R_c = R_r$	0.05	6.36	0.51	5.25	2.20
	0.10	6.59	0.54	5.11	2.40
	0.14	5.83	0.62	5.40	2.50
	0.30	3.52	0.94	10.55	4.85
$R_c = 0.85R_r$	0.07	7.63	0.56	5.55	3.27
	0.10	5.82	0.51	5.98	2.93
	0.15	6.88	0.73	8.78	4.73
	0.29	3.75	0.78	10.55	6.70

It should be noted that the overall decrease in on-rate constants between an $N = 1$ and $N = 2$ conformation is about two orders of magnitude (Table A1), making this the rate-limiting step of the entire binding process. This observation was also reported by Northrup and Erickson's protein-protein association model (Northrup & Erickson 1992). This is also supported in Table 1 (Chapter 2) by the fact that once the reactants have achieved an $N = 2$ conformation, 60% of the trajectories in an uncrowded case, and over 90% in a crowded case, remain partially bound and lead to an $N = 3$ conformation prior to diffusing apart— a much greater probability than $N = 0$ or 1 going to $N = 3$ for any

crowding scenario. Once in the $N = 2$ conformation, depletion forces again increase the probability of finishing the bond by biasing the reactants to not separate, and to rotate about this hinge-like partial bond until a complete bond is formed, although this is not the rate limiting step, so there is little is little difference in fold-change of k_{on} from $N = 2$ to $N = 3$.

Table A2. *Rates of arrival for reactants from 9nm to 4.2nm center-to-center.*

Crowding Molecules	ϕ	k_{DIFF} (μs^{-1})
	0	3.26
$R_c = 1.25R_r$	0.05	3.23
	0.08	3.22
	0.12	3.17
	0.29	2.14
$R_c = R_r$	0.05	3.16
	0.10	3.02
	0.14	2.89
	0.30	1.82
$R_c = 0.85R_r$	0.07	3.09
	0.10	2.81
	0.15	2.58
	0.29	1.70

Table A3. *Comparison of the model presented here with Northrup and Erickson's model.*

Stereospecificity	k_{on} **(**$M^{-1}s^{-1}$**)** (Northrup & Erickson 1992)	k_{on} **(**$M^{-1}s^{-1}$**)** Current model ($\phi = 0$)
$N = 0$ (Smoluchowski)	7×10^9	7.43×10^9
$N = 1$	3.8×10^8	5.52×10^8
$N = 2$	4×10^6	4.50×10^6
$N = 3$	2×10^6	2.18×10^6

Table A4. *Mean edge-to-edge separation distance of reactants during an encounter.*

Crowding Molecule	ϕ	Edge-to-Edge Separation (nm)
$R_c = 1.25R_r$	0	2.17
	0.29	1.70
$R_c = R_r$	0	1.79
	0.30	1.35
$R_c = 0.85R_r$	0	1.54
	0.29	1.16

Table A5. *Diffusion-limited (N = 0) and N = 1 off-rate results.*

Crowding Molecules	ϕ	$k_{off,0,1}$ (μs^{-1})	$K_{eq,0,1}$ (M^{-1})	$\Delta G^o_{0,1}$ ($k_B T$)
	0	18.45	402.85	-6.00
$R_c = 1.25R_r$	0.29	8.49	550.03	-6.31
$R_c = R_r$	0.30	6.12	508.85	-6.23
$R_c = 0.85R_r$	0.29	7.04	531.80	-6.28

It should be noted that, since it was assumed there was no energetic contribution for reactants in the $N = 1$ conformation, their dissociation was the same as for the $N = 0$ results, as seen in Table A5, above.

It is interesting to note that the equilibrium constant still increases for the diffusion-limited case, even though the on-rate constant decreases. This is because the extent to which the off-rate constant decreases is greater than the fold decrease in the on-rate constant for equivalent crowding scenarios. Thus, the addition of crowders (slightly) promotes net assembly for reactants with no stereospecific requirements (diffusion-limited) as seen by the small drop in $\Delta G^o_{0,1}$ in Table A5, above.

Surface Area Calculation

A fractional amount of surface area explored by a freely diffusing molecule over a given time interval, t_{enc}, can be found using

$$\delta S = \Omega R_r^2 \tag{A1}$$

where δS is an arbitrary, differential amount of surface area rotated in space during a rotation event, and

$$\Omega = 2\pi(1-\cos\Delta\theta) \quad [=] \quad \text{Steradians} \quad . \tag{A2}$$

The term $\Delta\theta$ can be found using the definition of the root-mean squared rotational displacement (RMSD) in three dimensional space, as

$$RMSD = \Delta\theta = \sqrt{6D_r < t_{enc} >} \quad . \tag{A3}$$

Substituting Eq. A2 and Eq. A3 into Eq. A1 yields an expression for determining a differential amount of surface area explored by a freely diffusing sphere, as

$$\delta S = 2\pi R_r^2 \left(1-\cos\sqrt{6D_r < t_{enc} >}\right) \quad . \tag{A4}$$

Dividing Eq. A4 by the total surface area of a sphere ($S_{TOT} = 4\pi R_r^2$) yields the fractional amount of surface area explored by a freely diffusing sphere in some average amount of time, $<t_{enc}>$, as in Eq. A5.

$$\frac{\delta S}{S_{TOT}} = \tfrac{1}{2}\left(1-\cos\sqrt{6D_r < t_{enc} >}\right) \tag{A5}$$

Table S6, below, shows the fold increases of explored surface area during an encounter for different crowding environments. Northrup and Erickson reported that

the rotational correlation time for the 1.8nm sphere is 5.3ns. Observing Table S6, it is evident that the addition of crowders brings the duration of an encounter (as defined in the Results and Discussion section) sufficiently close to the correlation time, thus enabling the reactants to almost completely rotationally reorient themselves during any given encounter, leading to the increase in probability of achieving the N = 3 conformation, thus increasing their on-rate constants.

Table A6. *Fractional surface area explored by a freely diffusing reactant in various crowding situations. Encounters were treated as defined in the Results & Discussion section in Chapter 2.*

Crowder Size	ϕ	$\langle t_{enc} \rangle$ **(ns)**	$\frac{\delta S}{S_{TOT}}$	**Fold Increase**
$R_c = 1.25R_r$	0	4.354	0.1922	1.1956
	0.29	5.284	0.2298	
$R_c = R_r$	0	4.050	0.1796	1.3179
	0.30	5.459	0.2367	
$R_c = 0.85R_r$	0	3.444	0.1542	1.2983
	0.29	4.550	0.2002	

Interaction Potentials in Crowded Solutions

Pairs of test molecules were initiated at an edge-to-edge distance of 2Å and underwent Brownian motion for 0.1 microseconds while the center-to-center separation distance between the pair was recorded at every step. To capture the energetic

landscape associated with the interaction potential between a pair of molecules as a function of radial separation distance, r, Boltzmann's relation was utilized, as

$$P(r) \propto \exp\left[-\Delta G_{DEP}/k_B T\right] \tag{A6}$$

where ΔG_{DEP} is the apparent free energy due to depletion effects, k_B is Boltzmann's constant, and T is the absolute temperature. The probability density function (PDF) of the distribution of their separation distances for each crowding case was normalized to the $\phi = 0$ crowding case, and this normalized distribution was entered into Eq. A6 as an estimation for $P(r)$, which is the probability of finding two spheres separated by a center-to-center distance, r (Yodh et al. 2001). Figure A1, below, shows the probability density functions of 1,000 molecular pair trajectories for various crowding scenarios. The shift (to the left) in the median separation distance between test molecule pairs (i.e. the peaks of each curve in the PDFs) is evidence for depletion forces biasing translational diffusion of the pair closer together once within the critical distance.

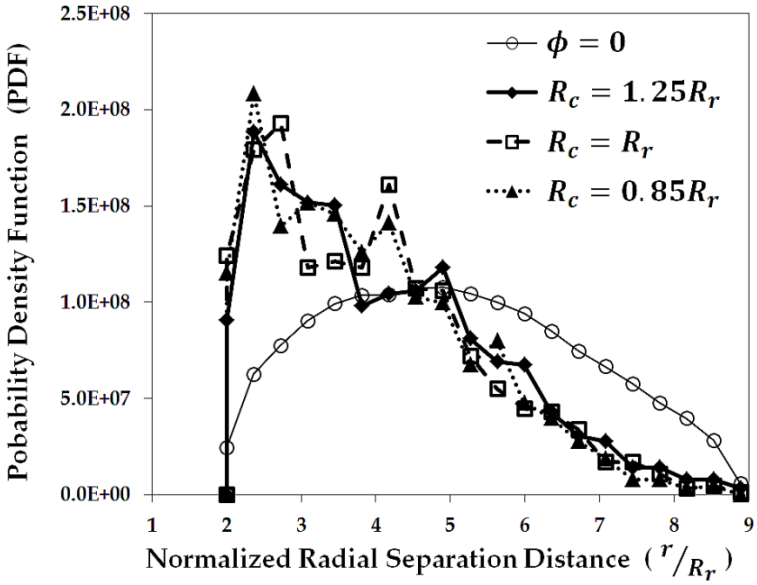

Figure A1. *Probability density functions for reactant separation distances in various crowded environments. Due to the hard-sphere assumption, reactants cannot be separated by a centroid separation distance less than r = 2Rr. It should also be noted that r = 9Rr approaches the dimension of the simulation domain, resulting in impossible separation distances as defined by this model.*

Dependence on potential energy curve

An interesting investigation of the model involved changing the potential well from that described in Eq. 14 and Figure 1f, to

$$U(N) = \begin{cases} \infty, & Overlap \\ -18.6k_BT, & N = 3,4 \\ -12.4k_BT, & N = 2 \\ -6.2k_BT, & N = 1 \\ 0, & N = 0, \end{cases} \tag{A7}$$

to determine the sensitivity of the shape of the potential to the effects of depletion forces due to crowding. The most important change in this potential curve is the addition of an energetic component to the N =1 conformation.

It was found that, with the modified potential well, the rate-limiting step in association (i.e. reaching N = 3) is no longer reaching the N = 2 conformation, but is now reaching the N = 1 conformation. This is evident in the fact that the probability of reaching an N = 2 conformation after having reached an N = 1 conformation is ~98%, whereas only ~30% of encounters ever reached the N = 1 case. Therefore, since reaching the N = 1 conformation (a much less stereospecific restriction than reaching the N = 2 conformation), the on-rate constants do not benefit as much from the increased encounter time (due to depletion forces) beyond what is required to achieve the rate-limiting step. This is evident in figure below in how the on-rate constants for the higher degrees of stereospecificity (i.e. N = 2 and 3) collapse onto that of the N = 1 conformation on-rate constant. Thus, the stereospecific requirement for the *rate-limiting step of association* is a key determinant in how reactions are affected by crowding.

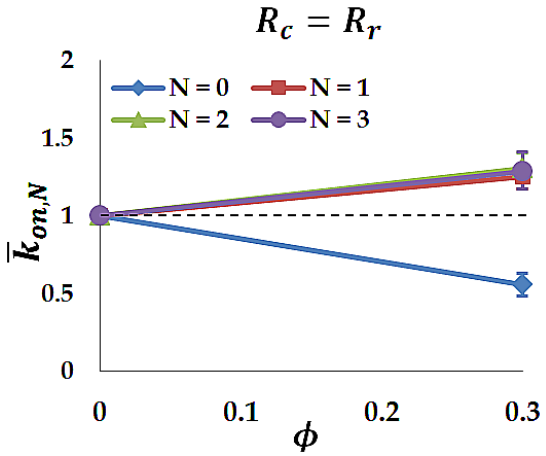

Figure A2. *Normalized on-rate constants as a function of crowder volume fraction (ϕ) for reactants with the modified potential well described in Eq. S7, where* $\bar{k}_{on,N} = k_{on,N}|_{\phi} / k_{on,N}|_{\phi=0}$. *Only the case where crowding and reactant molecules are of equal size was investigated, but similar trends can be expected for the range of crowder size investigated previously in this work.*